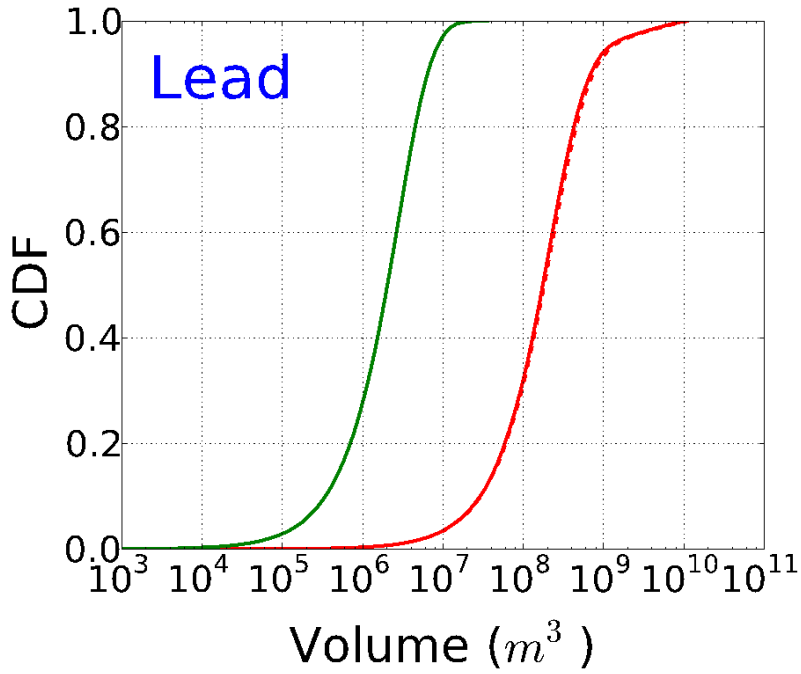

Reduced-Order Model for Estimating Impacts from CO_2 Storage Leakage to Alluvium Aquifers: Third-Generation, Combined Physical and Chemical Processes

6 October 2016

Office of Fossil Energy

NRAP-TRS-II-009-2016

Disclaimer

This report was prepared as an account of work sponsored by an agency of the United States Government. Neither the United States Government nor any agency thereof, nor any of their employees, makes any warranty, express or implied, or assumes any legal liability or responsibility for the accuracy, completeness, or usefulness of any information, apparatus, product, or process disclosed, or represents that its use would not infringe privately owned rights. Reference therein to any specific commercial product, process, or service by trade name, trademark, manufacturer, or otherwise does not necessarily constitute or imply its endorsement, recommendation, or favoring by the United States Government or any agency thereof. The views and opinions of authors expressed therein do not necessarily state or reflect those of the United States Government or any agency thereof.

This report (LLNL-TR-652828) has been reviewed by Lawrence Livermore National Laboratory and approved for public release.

Cover Illustration: Comparison of lead (green line) and pH (red line) volumes estimated from the hydrology reduced-order model (ROM), with those corrected for geochemical reactions in the protected groundwater (dashed-red line). Dashed red-line is superimposed on the red line.

Suggested Citation: Carroll, S. A.; Bianchi, M.; Mansoor, K.; Zheng, L.; Sun, Y.; Spycher, N.; Birkholzer, J. *Reduced-Order Model for Estimating Impacts from CO_2 Storage Leakage to Alluvium Aquifers: Third-Generation Combined Physical and Chemical Processes*; NRAP-TRS-II-009-2016; NRAP Technical Report Series; U.S. Department of Energy, National Energy Technology Laboratory: Morgantown, WV, 2016; p 44.

An electronic version of this report can be found at:
http://www.netl.doe.gov/research/on-site-research/publications/featured-technical-reports

https://edx.netl.doe.gov/nrap

Reduced-Order Model for Estimating Impacts from CO_2 Storage Leakage to Alluvium Aquifers: Third-Generation, Combined Physical and Chemical Processes

Susan Carroll[1], Marco Bianchi[2], Kayyum Mansoor[1], Liange Zheng[2], Yunwei Sun[1], Nic Spycher[2], Jens Birkholzer[2]

[1]Atmospheric, Earth and Energy Division, Lawrence Livermore National Laboratory, 7000 East Avenue, Livermore, CA 94551

[2]Earth Sciences Division, Lawrence Berkeley National Laboratory, 1 Cyclotron Road, Berkeley, CA 94720

NRAP-TRS-II-009-2016

Level II Technical Report Series

6 October 2016

This page intentionally left blank.

Table of Contents

EXECUTIVE SUMMARY **1**

1. INTRODUCTION **2**

2. IMPACT THRESHOLDS **3**

3. DEVELOPMENT OF THE HYDROLOGY ROM **5**
3.1 REACTIVE - TRANSPORT SIMULATIONS 6
3.2 CO_2 AND BRINE LEAKAGE 8
3.3 RESULTS – HYDROLOGY ROM 9

4. DEVELOPMENT OF THE CHEMICAL SCALING FUNCTION **12**
4.1 REACTIVE TRANSPORT SIMULATIONS 16
4.2 GEOCHEMICAL MODEL 18
4.3 CHEMICAL SCALING FACTOR RESULTS 23

5. RESULTS FROM THE INTEGRATED ROM FOR GROUNDWATER CHEMISTY **26**

6. EFFECTS OF WELLBORE MITIGATION ON PLUME VOLUME AND MIGRATION **30**

7. CONCLUSIONS **33**

8. REFERENCES **34**

This page intentionally left blank.

List of Figures

Figure 1: Flow chart of the third-generation of groundwater impacts modeling. 5

Figure 2: Schematic of the CO_2 and brine leakage model parameters and profiles in the generalized model. 9

Figure 3: Fidelity of pH, TDS, trace metal (lead as an example), and organic (benzene – Bz – as an example) ROMs to reproduce simulated data as a function of time. 11

Figure 4: Plumes for thresholds pH < 7 and Pb > 3.04×10-9 mol/L (0.63 µg/L) from one particular simulation, which considered all the chemical reactions.....14

Figure 5: Spatial distribution of Pb > 3.04×10-9 mol/L (0.63 µg/L) plume in the simulation, which is the same as the simulation shown in Figure 4 except that no chemical reaction is considered. 14

Figure 6: The leakage rate of CO_2 and brine as a function of time from Carroll et al. (2014). 17

Figure 7: Comparison between the values from numerical simulations and those emulated with the developed scaling functions: As (a), Ba (b), Cd (c), and Pb (d). 24

Figure 8: Comparison between the values from numerical simulations and those emulated with the developed scaling functions: benzene(a), naphthalene (b), and phenol (c). 25

Figure 9: Application of the scaling factors for arsenic, barium, cadmium, and lead (left column) to the hydrology ROM (right column) where the solid green line represents trace metal output from the hydrology ROM, the dashed red line represents the hydrology ROM corrected for geochemical reactions, and the solid red line represents the pH plume volume.....27

Figure 10: Application of the scaling factors g'(x) (left column) to the hydrology ROM (right column) where the solid and dashed lines represent the uncorrected and corrected plume volumes for benzene, naphthalene, and phenol. 28

Figure 11: Range of pH and TDS plume volumes estimated from the hydrology ROM. 29

Figure 12: Correlation of pH 7 and TDS 1,300 mg/L volumes with cumulative CO_2 and brine mass and mitigation time. 31

Figure 13: Example of pH (B) and TDS (C) plume evolution in plan view for given simulation (#682) with specific parameter input listed in (A). Color contours correspond to red = 10 years, orange = 40 years, yellow = 90, green = 135 years, cyan = 200 years. Solid circles show the location of shallow groundwater wells at this site. 32

List of Tables

Table 1: Initial aquifer concentrations used in the simulations and estimated mean aquifer values, and no-impact thresholds 4

Table 2: Parameter definition and ranges for hydrologic simulations and emulations....7

Table 3: Trace metals and organics concentrations considered in the protected groundwater simulations and ROM. Trace metals are based on experiments by Karamilidis et al. (2013) and organic concentrations are based on Zheng et al. (2010)....7

Table 4: Proposed parameter ranges for generalized CO_2 and brine leakage models 9

Table 5: Global correlation coefficients for the comparison of emulated and simulated plume volumes for pH, TDS, As, Ba, Cd, Cr, Fe, Mn, Pb, benzene, naphthalene, and phenol for impact thresholds....10

Table 6: Input parameters of the development of the scaling functions 15

Table 7: Initial chemical composition of groundwater in the model. Note that the concentration of Cl was somewhat modified from the original data to maintain charge balance. The Fe^{+3} concentration is calculated by assuming equilibrium with goethite....17

Table 8: Kinetic properties for minerals considered in the model (see text for data sources), “Primary” minerals are initially present in the aquifer. “Secondary” minerals are formed by precipitation. 19

Table 9: Equilibrium constants of the major rock forming minerals. Chemical reactions for the minerals in the first column are written as the chemical species in the first row with stoichiometric coefficients listed under each species. 20

Table 10: Cation exchange reactions and selectivity coefficients, using the Gaines-Thomas convention (Appelo and Postma, 1994) 20

Table 11: Surface sorption reactions for As, Cd, and Pb on goethite, illite, kaolinite, and montmorillonite (DLM = double layer model, CCM = constant capacitance model 21

Table 12: Correlation coefficients from linear correlations of scaling functions calculated from the simulations and emulations shown in Figures 7 and 8 23

Acronyms, Abbreviations, and Symbols

Term	Description
3-D	Three-dimensional
As	Arsenic
BTEX	benzene, toluene, ethylbenzene, and xylene-volatile aromatic compounds typically found in petroleum
CCM	Constant capacitance model
Cd	Cadmium
CO2-PENS	Integrated Systems/Process model for Simulating the Fate of CO_2
CO_2	Carbon dioxide
Cr	Chromium
dT_{2C}	Duration of the peak CO_2 flux
dT_{2B}	Duration of the transition between the maximum and final flux
dT_{3C}	Duration of the transition to zero CO_2 flux after injection has stopped
DLM	Double layer model,
DOE	Department of Energy
Fe	Iron
EPA	U.S. Environmental Protection Agency
LBNL	Lawrence Berkeley National Laboratory
LLNL	Lawrence Livermore National Laboratory
λq_{BRN}	final brine flux
m	Meter
mg/L	Milligrams Per Liter
Mn	Manganese
NAWQA	U.S. Geologic Survey National Water-Quality Assessment Program
NRAP	National Risk Assessment Partnership
NUFT	Non-Isothermal, Unsaturated and Saturated Flow and Transport Code
PAH	Poly-aromatic hydrocarbons
Pb	Lead
pH	$-\log\{H^+\}$
PSUADE	Computer code of Problem Solving environment for Uncertainty Analysis and Design Exploration
q_{CO2}	Peak CO_2 flux
q_{BRN}	Initial and maximum brine flux
R^2	Linear correlation coefficient
ROM	Reduced-order model
T_{1C}	Time needed to reach peak CO_2 flux
T_{1B}	Brine injection time
TDS	Total dissolved solids
TOUGHREACT	Reactive transport simulator
USGS	U.S. Geological Survey
µg/L	Micrograms per Liter

Acknowledgments

This work was completed as part of the National Risk Assessment Partnership (NRAP) project. Support for this project came from the U.S. Department of Energy's (DOE) Office of Fossil Energy's Crosscutting Research program. The authors wish to acknowledge Traci Rodosta (Carbon Storage Technology Manager), Kanwal Majajan (Carbon Storage Division Director), M. Kylee Rice (Project Manager), Mark Ackiewicz (Division of CCS Research - Program Manager), Susan Maley and Steve Seachman (NETL Strategic Center for Coal), and Regis Conrad (DOE Office of Fossil Energy) for programmatic guidance, direction, and support.

The authors also wish to acknowledge high performance computing at Lawrence Livermore National Laboratory and Yingqi Zhang for reviewing the report.

EXECUTIVE SUMMARY

The National Risk Assessment Partnership (NRAP) is developing a science-based toolset for the quantitative analysis of the potential risks associated with changes in groundwater chemistry from carbon dioxide (CO_2) injection. In order to address uncertainty probabilistically, NRAP is developing efficient, reduced-order models (ROMs) as part of its approach. These ROMs are built from detailed, physics-based process models to provide confidence in the predictions over a range of conditions. The ROMs are designed to reproduce accurately the predictions from the computationally intensive process models at a fraction of the computational time, thereby allowing the utilization of Monte Carlo methods to probe variability in key parameters.

This research developed ROMs that describe changes in diluted groundwater chemistry if CO_2 and brine were to leak into an overlying alluvium aquifer similar to the High Plains aquifer, Haskel County, Kansas, USA. The protocol allows uncertainty and variability in aquifer heterogeneity, fluid transport and geochemical reactions to be collectively evaluated to assess potential changes in groundwater pH, total dissolved solids (TDS), As, Ba, Cd, Pb, benzene, naphthalene, and phenol concentrations by developing a scaling function that can be applied to correct the output from the hydrology ROM for geochemical reactions. The hydrology ROM takes into account the uncertainties in brine and CO_2 leakage, aquifer heterogeneity and fluid transport, whereas the geochemical scaling function considers the uncertainties in chemical reactions. Inclusion of chemical correction increases trace metal plumes by 10 to 100 times, suggesting that CO_2 leakage leaches trace metals from the aquifer sediments and should be considered. Corrections are needed for other trace metals, such as chromium, iron, manganese, and zinc. In contrast to the observed increases in trace metal plume volumes, inclusion of bio-degradation greatly reduces plume volumes for organics.

Although a general protocol has been established for developing a ROM that can be used to assess groundwater impacts by including physical and chemical uncertainty and variability, model accuracy was not able to reach the $R^2 = 0.90$ goal in all cases. Correlation coefficients between emulations and simulation output range between $R^2 = 0.75$ to 0.85 for trace metals and about 0.60 for the organics. Improvements may be achieved by increasing the number of simulations to more fully sample the parameter space and by applying different mathematical forms for the chemical scaling function.

Better agreement between the hydrology pH and TDS ROMs at times less than 50 years is needed to assess near-term risks to leakage and to evaluate mitigation and monitoring plans. This will require a much finer mesh size to capture changes in groundwater chemistry from small amounts of CO_2 and brine leaked into the aquifer. Smaller mesh sizes may also be needed to improve the overall performance of the TDS ROM. The small TDS plume volumes yield ROMS that are only accurate to about 75% with the current mesh structure.

To make ROMs applicable for other alluvium aquifers, the authors recommend that ROMs be developed for variable thresholds since other aquifers are likely to have different background water chemistry in light of the “no net degradation” requirement in the U.S. Environmental Protection Agency (EPA) guidelines. The full chemical and hydrology ROMs developed here are specific to the output thresholds that define no net degradation to the High Plains aquifer. Variable threshold ROMs could be extracted from the same dataset used to develop the ROMs described herein.

1. INTRODUCTION

Carbon dioxide (CO_2) geologic storage is being considered as a possible measure to curb the anthropogenic emissions of greenhouse gases. A careful assessment of the risk associated with CO_2 geologic storage is critical to deployment of large scale CO_2 geological storage. One of the potential risks is the impact of potential CO_2 leakage from deep subsurface reservoirs on overlying groundwater aquifers. The leakage of CO_2 could affect such aquifers increasing the concentration of carbonic acid and causing pH to drop, by mobilizing trace elements through mineral dissolution, desorption, and/or exchange, and by increasing dissolved solids, trace metals, and organics directly from the leaking brine (e.g., Aiuppa et al., 2005; Zheng et al., 2009; Apps et al., 2010; Kharaka et al., 2010; Little and Jackson, 2010; Wilkin and Digiulio, 2010; Zheng et al., 2012; Trautz et al., 2012). Accurate prediction of groundwater impacts is complicated by uncertainty and variability in data, and key parameters are needed to describe leakage sources and the properties of aquifer systems. In principle, the full range of potential groundwater impacts could be assessed through rigorous numerical modeling, but a complete treatment of uncertainty and variability would be computationally prohibitive for most operators and regulators.

The National Risk Assessment Partnership (NRAP) is developing a science-based toolset for the analysis of the potential risks associated with changes in groundwater chemistry from CO_2 injection. This quantification approach is based on simulating coupled physical and chemical processes to predict how the natural system behaves over time, and it includes uncertainty quantification explicitly. In order to address uncertainty probabilistically, NRAP is developing efficient, reduced-order models (ROMs) as part of its approach. These ROMs are built from detailed, physics-based process models to provide confidence in the predictions over a range of conditions. However, the ROMs are designed to reproduce accurately the predictions from the computationally intensive process models at a fraction of the computational time, thereby allowing the utilization of Monte Carlo methods to probe variability in key parameters.

The development of ROMs that describe impacts to protected groundwater should consider all relevant physical flow and chemical processes. Developing ROMs based on high-fidelity numerical models that incorporate all relevant chemical reactions and transport fields is very challenging and computationally demanding. These difficulties are circumvented by correcting output from the hydrology ROM with chemical scaling functions derived from process models that are optimized for chemical reactions.

The natural system studied here is an alluvium aquifer consisting of layers of relatively high-permeable sands interbedded with low-permeable clays based on the hydrostratigraphic structure of the High Plains aquifer. Input parameters considered include: aquifer heterogeneity, permeability, porosity, regional groundwater flow, injection period, wellbore remediation, CO_2, total dissolved solids (TDS), trace metal leakage rates over time, and geochemical parameters. The hydrology ROM and the chemistry scaling function are specific to thresholds described in Section 2 that represent no net degradation to the groundwater quality. The hydrology ROM is derived from physics-based simulations accounting for heterogeneous transport conditions, carbonate buffering, and mitigation for leakage through a single wellbore and is described in Section 3. The chemistry scaling function corrects hydrology ROM output for relevant geochemical reactions and is described in Section 4. The impacts to groundwater chemistry are discussed in Section 5. Section 6 assesses the ability of natural recharge to restore groundwater quality of the protected resource.

2. IMPACT THRESHOLDS

The hydrology ROMs and chemical scaling functions generated in this study are specific to thresholds that represent no net degradation to the groundwater quality. The impact thresholds defined for pH, TDS, trace metals, and select organics in Table 1 represent concentrations above the background water chemistry. Each threshold was calculated as the 95%-confidence, 95%-coverage tolerance from data collected in a 2010 U.S. Geological Survey (USGS) groundwater survey of 30 wells within the High Plains aquifer from an area outside of lithology model site. This dataset was chosen because spatial and temporal data were not available from model site. Benzene, naphthalene, and phenol were considered as representative of: benzene, toluene, ethylbenzene, and xylene-volatile aromatic compounds typically found in petroleum (BTEX); poly-aromatic hydrocarbons (PAH), and phenol organic compounds that could be present in the leaking brine (Zheng et al., 2010). Table 1 also includes regulatory standards referring to concentrations that exceed primary or secondary maximum contaminant levels designated by the U.S. Environmental Protection Agency (EPA, 2009). Primary drinking water standards are for trace metals, such as, Ba, Cd, Cr, Cu, Pb, and BTEX organics among others, and are legally enforced for the protection of public health by limiting the levels of contaminants in drinking water. Secondary drinking water standards, which include standards for Fe, Mn, and Zn, are non-enforceable guidelines regulating contaminants that may cause cosmetic or aesthetic effects in drinking water. Currently PAHs and phenols are unregulated.

Table 1: Initial aquifer concentrations used in the simulations and estimated mean aquifer values, and no-impact thresholds

Parameter	Initial Value Used in Third-Generation Simulations	Mean of Selected and Adjusted 2010 Data[b]	Impact Threshold[c]	U.S. EPA Regulatory Standard
pH	7.6[a]	7.5[c]	7.0	6.5
TDS	570 mg/L[a,d]	440 mg/L[d]	1,300 mg/L[d,e]	500 mg/L[e]
Arsenic	1.500 µg/L	1.500 µg/L	9.300 µg/L	10.0 µg/L
Barium	43.000 µg/L [b]	43.000 µg/L [b]	140.000 µg/L	2,000 µg/L
Cadmium	0.059 µg/L	0.059 µg/L	0.250 µg/L	5 µg/L
Chromium	1.000 µg/L	1.000 µg/L	3.900 µg/L	100 µg/L
Iron	5.400 µg/L [b]	5.400 µg/L [b]	43.000 µg/L [b]	300 µg/L
Lead	0.086 µg/L	0.086 µg/L	0.630 µg/L	15 µg/L
Manganese	0.350 µg/L[d]	0.350 µg/L [d]	7.000 µg/L [d]	50 µg/L
Benzene	0	<0.030 µg/L [d]	0.030 µg/L [g]	5 µg/L
Naphthalene	0	<0.200 µg/L [d]	0.200 µg/L [g]	700 µg/L
Phenol	0	<0.003 µg/L [f]	0.003 µg/L [g]	10,000 µg/L [h]

(a) Based on Carroll et al. (2009)
(b) Geometric mean except for pH
(c) 95%-confidence, 95%-coverage tolerance limit based on log values except for pH
(d) Rounded to two significant digits
(e) Threshold value exceeds regulatory standard; using the regulatory standard may result in widespread false positives under field conditions
(f) As 4-Chloro-2-methylphenol
(g) Detection limit for the 2010 U.S. Geologic Survey National Water-Quality Assessment Program (NAWQA) sample data
(h) Recommended Water Quality Criteria for Human Health, consumption of Water + Organism (74 FR 27535); http://water.epa.gov/scitech/swguidance/standards/criteria/current/index.cfm#hhtable

3. DEVELOPMENT OF THE HYDROLOGY ROM

The hydrology ROM focused on variable wellbore leakage rates, mitigation times and arsenic, barium, cadmium, chromium, iron, lead, manganese, benzene, naphthalene, and phenol concentrations in the leaking brine, as well as uncertainty in the hydrologic properties of the protected groundwater. This section describes the reactive transport models, parameter variability, and leakage profiles used to build the ROM, as well as the fidelity of the resulting threshold-specific ROMs. PSUADE, an uncertainty quantification code (Tong, 2005, 2010) was used to establish sampling points for the reactive transport simulations, to conduct parameter sensitivity analysis, and to develop ROMs from the simulated results. The overall work flow is shown in Figure 1. Tables 2–4 list parameter ranges for development of the aquifer model, hydrologic flow, leakage flux, and brine concentrations. Note that flux is recalculated as cumulative CO_2 and brine mass to drive the hydrology ROM. The polynomial-based ROMs should be able to emulate the outcome of the numerical model but with less complexity, more thorough sampling of the parameter space, and significantly faster simulation times to generate risk-based profiles that can be used in decision making processes.

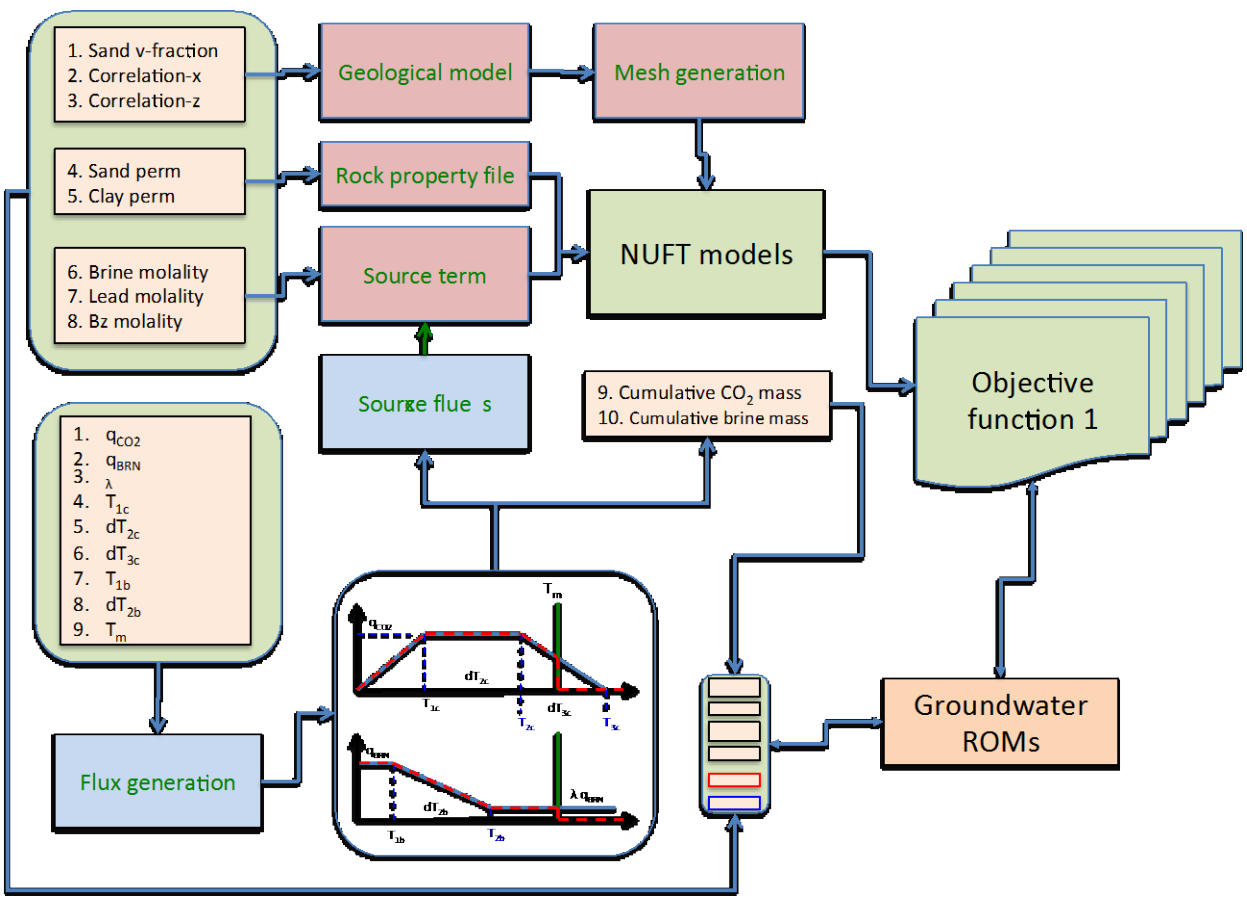

Figure 1: Flow chart of the third-generation of groundwater impacts modeling.

3.1 REACTIVE - TRANSPORT SIMULATIONS

The simulation of the protected groundwater response to leakage used the same protocol as was used in the development of the second aquifer ROMs, and is only briefly described here (Carroll et al., 2014).

The first step to developing the hydrology ROM is to build statistical models of the aquifer that account for the variability and uncertainty in the lithology. The natural system studied here was an alluvium aquifer consisting of layers of permeable sand interbedded with layers of clay with low permeability, and was based on the lithology of the High Plains aquifer. Material-volume fraction and correlation lengths derived from well log data were used to build 1,000 geostatistical models that contain 3-D distributions of high and low permeability zones for use in the reactive-transport simulations. PSUADE and TPROGS software were used to build the 3-D geological models (Tong, 2005, 2010; Carle, 1999). Each simulation uses a different geostatistical realization combined with other variable input to assess the impact of leakage on groundwater quality. Ranges over which the aquifer characteristics and brine chemistry were sampled are listed in Tables 2–4.

This study simulated the geochemical response of a protected groundwater to CO_2 and brine leakage through wells from a CO_2 storage reservoir using a multi-phase and multi-component reactive transport code called NUFT (Nitao, 1998; Hao et al., 2011). The numerical model domain extended to 10,000 m × 5,000 m × 240 m (x, y, z) with one leakage source placed at a depth of 198 m. Regional groundwater flow was maintained by a 0.3% hydraulic gradient, with constant-pressure boundary set on ground surface and at the aquifer bottom to maintain saturated and unsaturated zones. This model employed a variably spaced mesh with the smallest elements located at the injector with a total of 190,350 nodes. The mesh spacing ranged from 50 m to 152.7 m in the x-direction, 50 m to 154.5 m in the y-direction, and fixed at 4.8 m in the z-direction. Each simulation was executed for 20–60 hrs each using the high performance computing facility at Lawrence Livermore National Laboratory (LLNL).

A limited amount of chemistry was included to account for changes in groundwater pH due to CO_2 dissolution, dissolved sodium, and chloride as indicators of TDS, and total dissolved trace metal and organic concentrations from the leaking brine. The dissolution of CO_2 in groundwater promotes the following sets of reactions:

$$CO_2(g) \leftrightarrow CO_2(aq) \tag{1}$$

$$CO_2(aq) + H_2O \leftrightarrow HCO_3^- + H^+ \tag{2}$$

$$CaCO_3(calcite) + H^+ \leftrightarrow Ca^{2+} + HCO_3^- \tag{3}$$

These reactions promote the acidification of the system, which is then buffered by calcite dissolution. The resulting trace metal and organic plumes will be corrected by the scaling factor to account for relevant geochemical reactions (see Section 4). Background pH, TDS, and trace metal and organic concentrations in the aquifer are listed in Table 1 and are based on mean values reported for the regional aquifer in 2010, new analysis, and previous literature values (Last et al., 2013; Carroll et al., 2009).

Table 2: Parameter definition and ranges for hydrologic simulations and emulations

	Parameter	Minimum	Maximum	Unit
1	Sand volume fraction	0.35	0.65	-
2	Correlation length in X-direction	200	2500	[m]
3	Correlation length in Z-direction	0.5	25	[m]
4	Permeability in sand	-14	-10	$Log_{10}[m^2]$
5	Permeability in clay	-18	-15	$Log_{10}[m^2]$
6	Sodium molality	-3	1	$Log_{10}[mol\ kg^{-1}]$
7	Trace metal molality			See Table 3
8	Organic molality			See Table 3
9	CO_2 and brine flux			See Table 4

Table 3: Trace metals and organics concentrations considered in the protected groundwater simulations and ROM. Trace metals are based on experiments by Karamilidis et al. (2013) and organic concentrations are based on Zheng et al. (2010)

	Trace Metal	Minimum	Maximum	Unit
7	Arsenic	-7.98	-5.87	$Log_{10}[mol\ kg^{-1}]$
7	Barium			$Log_{10}[mol\ kg^{-1}]$
7	Cadmium	-8.87	-6.43	$Log_{10}[mol\ kg^{-1}]$
7	Chromium	-6.42	-4.02	$Log_{10}[mol\ kg^{-1}]$
7	Iron	-6.07	-2.79	$Log_{10}[mol\ kg^{-1}]$
7	Lead	-8.12	-4.74	$Log_{10}[mol\ kg^{-1}]$
7	Manganese	-5.13	-2.10	$Log_{10}[mol\ kg^{-1}]$
8	Benzene	-10	-3.2	$Log_{10}[mol\ kg^{-1}]$
8	Naphthalene	-10	-3.7	$Log_{10}[mol\ kg^{-1}]$
8	Phenol	-10	-4.1	$Log_{10}[mol\ kg^{-1}]$

3.2 CO_2 AND BRINE LEAKAGE

A generalized flux model was used to span a large range of CO_2 and brine input fluxes that could be transported from a pressurized reservoir and through a borehole and into the protected groundwater. The generalized model is not site specific and considers a range of CO_2 injection periods, wellbore permeability, and wellbore mitigation times. As such, the resulting groundwater ROMs should be transferable to other sites with similar water quality thresholds. The generalized CO_2 and brine leakage models were based on the results of 48,000 numerical wellbore simulations driven by reservoir pressure and saturation profiles coupled with wellbore permeability to yield CO_2 and complimentary brine leakage functions. The resulting leakages models and variable parameters are illustrated in Figure 2. Conceptually, CO_2 fluxes increase to a plateau during the onset of CO_2 injection into the storage reservoir, maintain a constant flux during injection, and then decrease overtime to some minimal level. Variability in the CO_2 leakage profile was generated using four parameters:

- q_{CO2} – the peak flux
- T_{1C} – the time needed to reach peak flux
- dT_{2C} – the duration of the peak flux
- dT_{3C} – the duration of the transition to zero flux after injection has stopped

Brine leakage profiles are different from that of CO_2. Brine leakage was characterized with a maximum and constant flux during injection, which falls off to a final flux after injection stops. Uncertainty in the brine leakage profile was generated using four parameters:

- q_{BRN} – the initial and maximum flux
- λq_{BRN} – the final flux
- T_{1B} – the injection time
- dT_{2B} – the duration of the transition between the maximum and final flux

An additional parameter, T_M, was included to represent wellbore mitigation time. This parameter was introduced to investigate the ability of natural recharge to restore groundwater quality of the protected resource and will be discussed in Section 6. The generalized flux is recast into two parameters that capture variations in cumulative CO_2 and brine leaked into the protected groundwater.

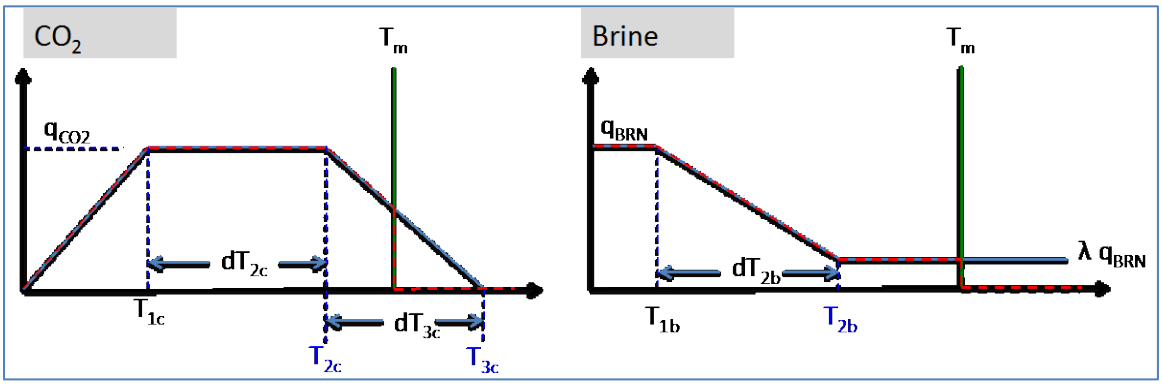

Figure 2: Schematic of the CO_2 and brine leakage model parameters and profiles in the generalized model.

Table 4: Proposed parameter ranges for generalized CO_2 and brine leakage models

Parameter	Min	Max	Notes
q_{CO2}	-3.000	-0.301	Log_{10} (0.001 – 0.5) kg s^{-1}
q_{BRN}	-2.301	-1.125	Log_{10} (0.005 – 0.075) kg s^{-1}
λ	0.200	0.300	Ratio for brine-leakage tail
T_{1c}	5.000	50.000	yr
dT_{2c}	0	100.000	yr
dT_{3c}	5.000	50.000	yr
T_{1b}	1.000	50.000	yr
dT_{2b}	1.000	10.000	yr
T_m	50.000	200.000	Mitigation time, yr

3.3 RESULTS – HYDROLOGY ROM

The ability of the emulations to reproduce the simulated results for specific thresholds for pH, TDS, As, Ba, Cd, Cr, Fe, Mn, Pb, benzene, naphthalene, and phenol was evaluated using global and time-based correlation coefficients (Table 5). The global correlations directly compare ROM and simulation output of all output times. Globally, the third-generation ROMs for pH, trace metals, and organics are robust and yield R^2 between 0.9 and 0.99. This is not the case for TDS with global $R^2 \approx 0.74$. At the time of writing this report it is not clear why the TDS ROM was less accurate than the simulations. Incorporation of the TDS ROM as part of the larger systems analysis should include the uncertainty in its overall performance.

Likewise, utilization of the ROMs over short time periods should be done with caution. Figure 3 shows emulation performance as a function of time. The emulations do not reproduce the simulated pH result to within 90% at times less than about 40 years. A similar time-dependent trend is observed for the TDS ROMs, but with a greater overall uncertainty. Trace metal and organic ROMs appear to be more robust and capture the simulated results after 2 to 5 years.

As was the case in the first and second-generation results, there is strong correlation between CO_2 mass and pH plume volume, with a secondary dependence on mitigation time, which also correlates with cumulative mass of the leak. Correlations for the TDS, trace metal, and organic plume volumes on brine mass are more variable than pH volume because they are also dependent on brine concentration.

Table 5: Global correlation coefficients for the comparison of emulated and simulated plume volumes for pH, TDS, As, Ba, Cd, Cr, Fe, Mn, Pb, benzene, naphthalene, and phenol for impact thresholds.

Parameter	U.S. EPA Regulatory Standard	R^2	Impact Threshold	R^2
pH	6.5	0.925	7.0	0.901
TDS	500 mg/l[e]	NA	1,300 mg/l	0.747
Arsenic	10 µg/l	0.986	9.300 µg/l	0.983
Barium	2000 µg/l	0.986	140.000 µg/l	0.946
Cadmium	5 µg/l	0.995	0.250 µg/l	0.962
Chromium	100 µg/l	0.922	3.900 µg/l	0.857
Iron	300 µg/l	0.987	43.000 µg/l	0.972
Lead	15 µg/l	0.991	0.630 µg/l	0.924
Manganese	50 µg/l	0.991	7.000 µg/l	0.986
Benzene	5 µg/l	0.974	0.030 µg/l	0.983
Naphthalene	700 µg/l	0.977	0.200 µg/l	0.980
Phenol	10,000 µg/l	0.972	0.003 µg/l	0.985

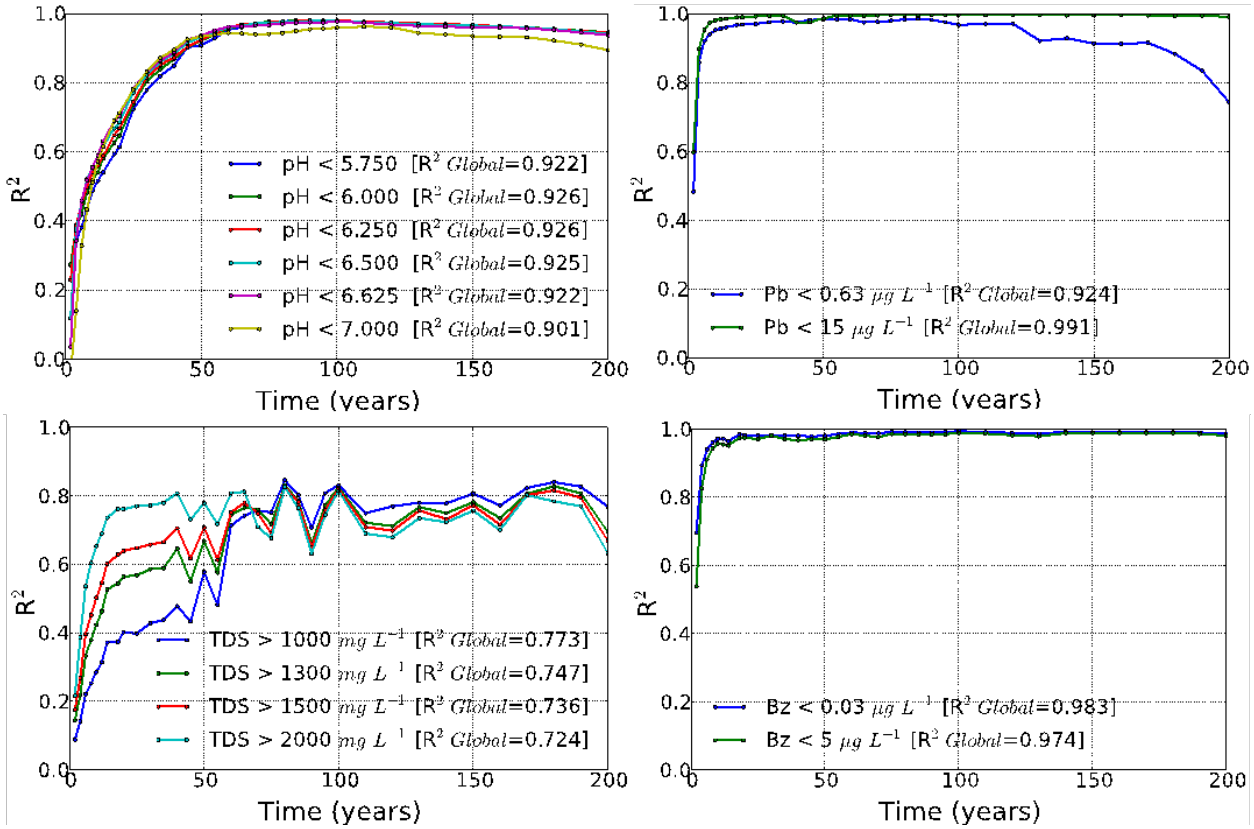

Figure 3: Fidelity of pH, TDS, trace metal (lead as an example), and organic (benzene – Bz – as an example) ROMs to reproduce simulated data as a function of time.

4. DEVELOPMENT OF THE CHEMICAL SCALING FUNCTION

This section describes the development of the chemical scaling function that is used together with the hydrology ROM to estimate impact of leakage for trace metals and organics in the protected groundwater. The chemical scaling function includes chemical processes that account for distribution of trace metals between groundwater and aquifer minerals and the degradation of organic contaminants, all of which depend on changes in pH, salt concentrations, and redox potential associated with the leaking CO_2 and brine.

The chemical scaling function is used to correct response of the hydrology ROM to more accurately estimate the impact of leakage on groundwater trace metal and organic concentrations. Scaling functions are derived by comparing the output of models with variable-fidelity and are used to better emulate the response of an original high-fidelity model. The approach is known as "variable-fidelity" or "multi-fidelity" modeling. Scaling functions can assume different functional forms including polynomials (e.g., Madsen and Langthjem, 2001; Viana et al., 2009; Sun et al., 2010), as well as of more flexible relationships such as kriging (Huang et al., 2006; Forrester et al., 2007) and neural networks (Kim et al., 2007). In contrast to traditional response surface ROMs, variable-fidelity ROMs are expected to better extrapolate the complex model response in unexplored regions of the input parameter space (Razavi et al., 2012). The second advantage, which is fundamental for this work, is that scaling functions are only minimally affected by the problem of dimensionality which limits the application of response surface surrogates to problems with a large number of input parameters (e.g., Koch et al., 1999). This is because their response is physically based and therefore their development requires a lower number runs of the original complex model.

Scaling functions can be multiplicative or additive depending on if the ratio rather than the difference between the responses from the lower and high-fidelity models is considered. This study found that the multiplicative approach provided the best accuracy when the scaling function $g(\mathbf{x})$ was defined as:

$$g(\mathbf{x}) = \frac{V_{HFM}(\mathbf{x})}{V_{LFM}(\mathbf{x}^*)} \tag{4}$$

where V_{HFM} is the output volume calculated with the high-fidelity model with $\mathbf{x}$ input parameters and V_{LFM} is the corresponding volume obtained with a lower-fidelity model with $\mathbf{x}^*$ input parameters. To ensure the correspondence between the two models outputs, V_{LFM} and V_{HFM}, $\mathbf{x}^*$ must be a subset of $\mathbf{x}$. The exact form of the scaling function $g(\mathbf{x})$ is typically unknown, especially for complex responses that depend on several physical and chemical processes such as those considered in this work. However, if an approximation of the scaling function based on a relatively limited number of runs of the high- and low-fidelity models can be found, V_{HFM} can then be approximated as:

$$\tilde{V}(\mathbf{x}) = V_{LFM}(\mathbf{x}^*) \cdot \tilde{g}(\mathbf{x}) \tag{5}$$

Where $\tilde{V}(x)$ is the emulated volume, and $\tilde{g}(x)$ is the approximated scaling function designed to correct the value V_{LFM}. In this work, $V_{LFM}(\mathbf{x}^*)$ is the output from a simulation that does not consider geochemistry (i.e., the hydrology ROM) and $\tilde{V}(x)$ is the corresponding output when all the relevant geochemical processes are taken into account. To estimate the latter output, reactive transport simulations were performed based on the geochemical model described in Section 4.2. The process of developing the approximate scaling function is analogous to the development of a traditional response surface ROM. However, scaling functions are generally less complex than typical response surface ROMs because their only purpose is to scale output derived from a similar model (Razavi et al., 2012).

Scaling functions for As, Ba, Cd, Pb, benzene, naphthalene, and phenol were developed using the thresholds listed in Table 1. Scaling functions for pH and TDS were not necessary because carbonate geochemistry, included in the hydrology ROM, accounts for the dominate changes in pH; and because mineral dissolution does not significantly alter the TDS estimated from brine leakage. To generate a scaling function for each of these outputs, a two-step procedure was followed and a GNU Octave v.3.6.4 script was written for this purpose. The first step designed a numerical experiment to perform multiple runs of a model with no chemistry (so-called low-fidelity model, and is similar to the physics-based process models that are used to generate hydrology ROM) and a model with chemistry (so-called high-fidelity model) with the hydrology and geochemical input. The input parameter space of the numerical models was sampled with a quasi-random sequence (LPτ) to generate 1,024 sample points assuming a uniform distribution for all the input parameters. The simulated time period (0–200 years) was sampled at 10-year intervals. Details on parameter ranges are given in Table 6. Note that the distribution and ranges of the hydraulic parameters are similar to those used in previous generations of the hydrology ROMs (Carroll et al., 2014). In step two, an approximation of the true scaling function (Equation 1) was estimated for each of the considered outputs. These approximated scaling functions $\tilde{g}(\mathbf{x})$ are polynomical and are used to correct the output from the model without chemistry (Equation 2). In this step, least-square fitting was applied to calculate the coefficients of the polynomials representing the scaling functions. In general, a third-order polynomial provided the best match between the numerical and emulated ratios for metals, while second-order polynomial provided more accurate fitting for organic compounds.

Scaling functions for trace metals were developed from ratios of $V_{TM\text{-}HFM}$ to $V_{pH\text{-}LFM}$ because of observed correlations between trace metal and pH plume volumes. Correlations were observed not only for As, Cd and Pb whose uptake reactions are known to be pH-dependent, but also for Ba, whose release is driven by Ca exchange at mineral surfaces (Zheng et al., 2012). The indirect correlation for Ba with pH is caused by the pH-dependence of calcite dissolution. Figure 4 compares the spatial distribution of pH and Pb plumes from one particular simulation, which considers all chemical reactions. The two plumes have similar distributions because pH and Pb concentrations are controlled by changes in acidity from CO_2 solubility. In the absence of geochemical reactions, the Pb volume is smaller in this example, because the Pb plume volume depends only on the transport of the amount of lead leaked from the reservoir and does not account for the amount of lead released from the aquifer sediments (Figure 5). Robust scaling parameters must be tied to pH to account for the chemical processes that ultimately control their concentrations from both leakage sources.

Scaling functions for organic compounds were developed from ratios of $V_{Org\text{-}HFM}$ to $V_{org\text{-}LFM}$ because the brine is the only source of organic compounds, and adsorption and oxidation reactions occur within the brine.

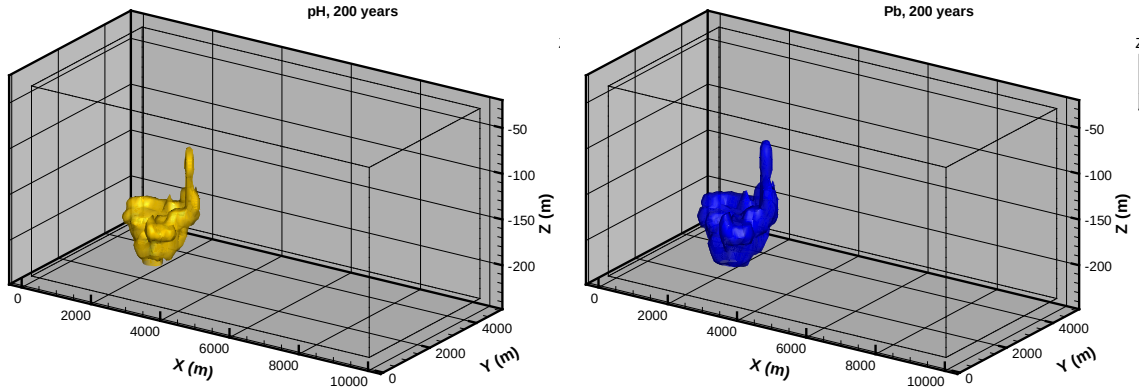

Figure 4: Plumes for thresholds pH < 7 and Pb > 3.04×10-9 mol/L (0.63 µg/L) from one particular simulation, which considered all the chemical reactions.

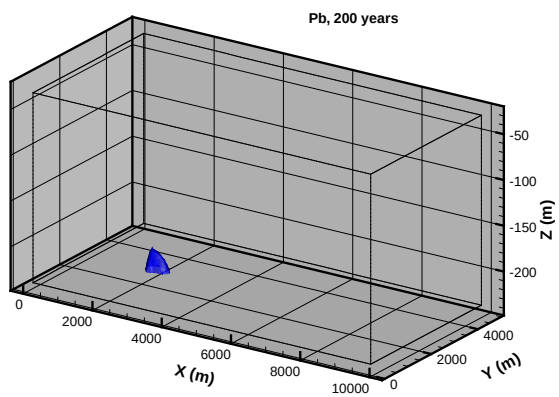

Figure 5: Spatial distribution of Pb > 3.04×10-9 mol/L (0.63 µg/L) plume in the simulation, which is the same as the simulation shown in Figure 4 except that no chemical reaction is considered.

Table 6: Input parameters of the development of the scaling functions

Parameter	Range
Porosity	0.25 to 0.50
Rock density (kg/m^3)	1500 to 2500
Sand permeability (m^2)	-14 to -10*
Van Genuchten parameter (m)	0.52 to 0.79
Van Genuchten parameter alpha (m^{-1})	-4.69 to -3.81*
Pb concentration in the leaking brine (mol/L)	-8.5 to -5.0*
Cd concentration in the leaking brine (mol/L)	-9.0 to -6.0*
As concentration in the leaking brine (mol/L)	-9.0 to -5.0*
Ba concentration in the leaking brine (mol/L)	-5.1 to -2.3*
Cl concentration in the leaking brine (mol/L)	-2.0 to -0.73*
Calcite volume fraction	0.0 to 0.2
Goethite volume fraction	0.0 to 0.2
Illite volume fraction	0.0 to 0.3
Kaolinite volume fraction	0.0 to 0.2
Montmorillonite volume fraction	0.0 to 0.5
Cation exchange capacity (CEC meq/100)	0.1 to 40.0
Benzene concentration in the leaking brine (mol/L)	-10.0 to -3.2*
Phenol concentration in the leaking brine (mol/L)	-10.0 to -3.7*
Naphtalene concentration in the leaking brine (mol/L)	-10.0 to -4.1*
Benzene distribution coefficient (L/kg)	-4.5 to 0.69*
Phenol distribution coefficient (L/kg)	-6.0 to 0.15*
Naphtalene distribution coefficient (L/kg)	-3.1 to 1.98*
Benzene degradation constant (1/s)	0 to -6.1 *
Phenol degradation constant (1/s)	0 to -5.63 *
Naphtalene degradation constant (1/s)	0 to -6.45*
Time (years)	0 to 200

*indicates log10 values

4.1 REACTIVE TRANSPORT SIMULATIONS

A single geostatistical realization of the aquifer lithology originally derived for the hydrology simulations (see Section 3.1**)** and a single CO_2 and brine leakage profile was used for reactive transport simulations. This is a reasonable approach because plume volumes are most sensitive to the cumulative mass of CO_2 and brine. There are four classes of parameters listed in Table 6 representing variability in hydrology, the concentration of leaking brine, the volume fraction of specific minerals included in the geochemical reactions, and degradation constants for the organics. Variability in hydrology and leak concentrations was required to correct the hydrology ROM for geochemical reactions (see Section 4.2). Geochemical variability was represented by adjustment of the amount of specific minerals, a key uncertainty. Mineral equilibrium and kinetic constants were fixed using published values (see Section 4.2). Note that the chemical ROM was developed for As, Ba, Cd, Pb, benzene, naphthalene, and phenol to demonstrate the processes on a reasonable number of key constituents.

Reactive-transport simulations were conducted with TOUGHREACT (Xu et al., 2011) and used the same domain size, boundary conditions, and hydrological gradient described in Section 3.1 with a refined mesh near the leakage source and a courser mesh in the far field for a total of 31,321 grid blocks. Leakage occurred at a single point (x = 2,000 m, y = 2,500 m, z = 250 m) with representative CO_2 and brine leakage profiles for a deep well that connects a geologic storage reservoir to a protected groundwater (Figure 6). These profiles represent median fluxes and allow the pH and salt dependence of geochemical reactions to be assessed and then scaled to the hydrology ROM. About 500 simulations were conducted to account for the uncertainties of both flow and chemical parameters.

The initial solution chemistry used in the model is listed in Table 7 and represents the arithmetic average of major and trace inorganic elements data collected in two surveys in 1999 and 2010 as part of the High Plains Regional Ground-Water Study conducted by the USGS's National Water-Quality Assessment Program (Becker et al., 2002). The surveys represent analyses of 30 to 74 randomly selected wells. A very small value was assigned to the initial concentration of benzene, phenol, and naphthalene because their concentrations were all below the detection limits in the 2010 survey.

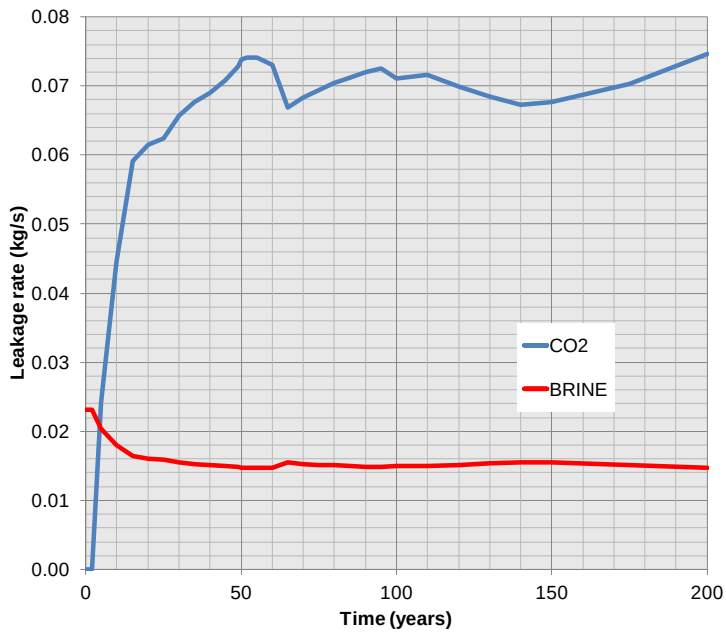

Figure 6: The leakage rate of CO_2 and brine as a function of time from Carroll et al. (2014).

Table 7: Initial chemical composition of groundwater in the model. Note that the concentration of Cl was somewhat modified from the original data to maintain charge balance. The Fe^{+3} concentration is calculated by assuming equilibrium with goethite.

Primary Species	Total Concentration (molal)	Primary Species	Total Concentration (molal)
Ca^{+2}	1.37E-03	$Sb(OH)_3(aq)$	5.59E-10
Mg^{+2}	8.74E-04	$H_3AsO_3(aq)$	2.33E-08
Na^{+}	1.60E-03	Ba^{+2}	8.10E-07
K^{+}	1.13E-04	Cd^{+2}	6.91E-10
Cl^{-}	1.85E-03	Pb^{+2}	1.57E-09
HS^{-}	6.48E-04	Benzene	1E-15
SO_4^{-2}	5.77E-05	Phenol	1E-15
HCO_3^{-}	3.95E-03	Naphthalene	1E-15
$H_4SiO_4(aq)$	5.33E-04	HSe^{-}	5.34E-08
Fe^{+2}	1.01E-06	Eh	-0.26 volts
Fe^{+3}	8.97E-16	pH	7.4
AlO_2^{-}	1.57E-07		

4.2 GEOCHEMICAL MODEL

The geochemical model is extensive and includes over 70 aqueous species, dissolution and precipitation kinetics for 14 minerals, 5 cation exchange reactions, 36 sorption reactions, and oxidation kinetics for 3 organics. Kinetic constants, mineral, cation exchange, and sorption mass balance reactions and constants are summarized in Tables 8–11. Equilibrium constants for aqueous complexes and minerals are taken primarily from THERMODDEM database (Blanc et al., 2012) which can be downloaded from the website: http://THERMODDEM.brgm.fr/index.asp. For those reactions that are not listed in THERMODDEM, thermodynamic data are taken from data0.ymp.r5 in the EQ3/6 V8.1 geochemical modeling package (Wolery, 1993) and Birkholzer et al., (2008). Cation exchange reactions are included for Na, K, Ca, Mg, and Ba as are surface complexation reactions for As, Cd and Pb on goethite, illite, kaolinite and montmorillonite. Surface complexation reactions on calcite are not considered in the model because calcite is a much weaker adsorbent in comparison with goethite, illite, kaolinite and montmorillonite and thus unlikely has significant impact on the adsorption of metals. Kinetic rate parameters for most rock-forming minerals were taken from Palandri and Kharaka (2004), which are based mainly on experimental studies conducted under far-from-equilibrium conditions. The overall rate equation is tied to mineral equilibria through Q/K with a pH dependent rate consisting of acid, neutral, and base mechanisms as indicated below:

$$r = \pm k\,A\left[1-\left(\frac{Q}{K}\right)^{\theta}\right]^{\eta}$$

and

$$k = k_{25}^{nu}\exp\left[\frac{-E_a^{nu}}{R}\left(\frac{1}{T}-\frac{1}{298.15}\right)\right] + k_{25}^{H}\exp\left[\frac{-E_a^{H}}{R}\left(\frac{1}{T}-\frac{1}{298.15}\right)\right]a_H^{n_H} + k_{25}^{OH}\exp\left[\frac{-E_a^{OH}}{R}\left(\frac{1}{T}-\frac{1}{298.15}\right)\right]a_{OH}^{n_{OH}}$$

where r is the kinetic rate, k is the rate constant, A is the specific reactive surface area, K is the equilibrium constant for the mineral–water reaction, and Q is the reaction quotient. Superscripts *nu*, *H*, and *OH* stand for the neutral, acid, and base mechanisms; E_a is activation energy that accounts for the dependence of the rate on temperature; T is absolute temperature, a_H and a_{OH} are hydrogen and hydroxyl ion activity; and n is an empirical constant. The parameters θ and η are assumed equal to unity. The mineral reactive-surface areas were taken from Xu et al. (2006), based on the work of Sonnenthal et al. (2005). A thorough review and discussion of the kinetic rates for arsenian pyrite, pyrite, and galena was given in Zheng et al. (2009). Oxidation of the organics was calculated with the first-order degradation kinetics:

$$\frac{dC}{dt} = -KC$$

Where C is the concentration of the organic compound, K is the first-order rate constant which was treated as a variable parameter.

Table 8: Kinetic properties for minerals considered in the model (see text for data sources), "Primary" minerals are initially present in the aquifer. "Secondary" minerals are formed by precipitation.

Mineral	A (cm^2/g)	Parameters for Kinetic Rate Law							
		Neutral Mechanism		Acid Mechanism			Base Mechanism		
		k_{25} $mol/m^2/s$	E_a KJ /mol	k_{25}	E_a	$n(H^+)$	k_{25}	E_a	$n(OH^-)$
Primary:									
Calcite	3.05	1.6×10^{-6}	62.76						
Illite	151.60	1.66×10^{-13}	35.00	1.05×10^{-11}	23.60	0.34	3.02×10^{-17}	58.9	-0.40
Kaolinite	151.60	6.91×10^{-14}	22.20	4.89×10^{-12}	65.90	0.78	8.91×10^{-18}	17.9	-0.47
Smectite	151.60	1.66×10^{-13}	35.00	1.05×10^{-11}	23.60	0.34	3.02×10^{-17}	58.9	-0.4
Goethite	12.90	2.51×10^{-15}	66.20	4.07×10^{-10}	66.20	1.00			
Albite	9.80	3.89×10^{-13}	38.00	8.71×10^{-11}	51.70	0.50	6.31×10^{-12}	94.1	-0.82
Quartz	9.80	3.98×10^{-14}	87.7						
K-feldspar	9.80	3.89×10^{-13}	38.00	8.71×10^{-11}	51.70	0.50	6.31×10^{-12}	94.1	-0.82
Secondary:									
Dolomite	12.90	2.95×10^{-8}	62.76	2.34×10^{-7}	43.54	1.00			
Magnesite	9.80	4.57×10^{-10}	23.50	4.17×10^{-7}	14.40	1.00			
Dawsonite	9.80	3.89×10^{-13}	38.00	8.71×10^{-11}	51.70	0.50	6.31×10^{-12}	94.1	-0.82
Muscovite	9.80	3.89×10^{-13}	38.00	8.71×10^{-11}	51.70	0.50	6.31×10^{-12}	94.1	-0.82
Gibbsite	9.80	3.89×10^{-13}	38.00	8.71×10^{-11}	51.70	0.50	6.31×10^{-12}	94.1	-0.82
Pyrite	12.90	2.52×10^{-12}	62.76						

Table 9: Equilibrium constants of the major rock forming minerals. Chemical reactions for the minerals in the first column are written as the chemical species in the first row with stoichiometric coefficients listed under each species.

Minerals	logK (25 °C)
Calcite + H^+ = Ca^{+2} + HCO_3^-	1.853
Illite + 6.3 H_2O = H^+ + 0.25Mg^{+2} + 0.85K^+ +3.4 H_4SiO_4(aq)+ 2.35AlO_2^-	-43.490
Kaolinite +3H2O = 2H+ +2H_4SiO_4(aq)+ 2AlO_2^-	-39.262
Smectite + 7.32 H_2O = 0.68H^+ + 0.17Ca^{+2} + 0.335Mg^{+2} + 3.99 H_4SiO_4(aq)+ 1.68AlO_2^-	-32.834
goethite + 3H^+ = 2H_2O + Fe^{+3}	0.363
Albite + 6H_2O = Na^+ + 3H_4SiO_4(aq)+ AlO_2^-	-20.126
Quartz +2H_2O = H_4SiO_4(aq)	-3.740
K-Feldspar + 6H_2O = K^+ + 3H_4SiO_4(aq)+ AlO_2^-	-22.394
Dolomite + 2H^+ = Ca^{+2} + Mg^{+2} + HCO_3^-	3.545
Magnesite + H^+ = Mg^{+2} + HCO_3^-	1.420
Dawsonite = H^+ + Na^+ + HCO_3^- + 2.35AlO_2^-	-18.535
Muscovite + 6H_2O =2H^+ + K^+ + 3H_4SiO_4(aq)+ 3AlO_2^-	-57.264
Ferrihydrite + 3H^+ = 3H_2O + Fe^{+3}	3.404
Gibbsite = H_2O + H^+ + AlO_2^-	-15.129

Table 10: Cation exchange reactions and selectivity coefficients, using the Gaines-Thomas convention (Appelo and Postma, 1994)

Cation Exchange Reaction	$K_{Na/M}$
Na^+ + X-H = X-Na + H^+	1
Na^+ + X-K = X-Na + K^+	0.2
Na^+ + 0.5X-Ca = X-Na + 0.5Ca^{+2}	0.4
Na^+ + 0.5X-Mg = X-Na + 0.5Mg^{+2}	0.6
Na^+ + 0.5X-Ba = X-Na + 0.5Ba^{+2}	0.2

Table 11: Surface sorption reactions for As, Cd, and Pb on goethite, illite, kaolinite, and montmorillonite (DLM = double layer model, CCM = constant capacitance model)

Reactions	Log k_{int}	Site Density mol/m^2	Surface Area m^2/g	Type of SCM Model	Reference
Goethite					
$goe^1_OH_2^+ = goe^1_OH + H^+$	-7.38	3.9-e8	80	DLM	1
$goe^1_O^- + H^+ = goe^1_OH$	10.74	3.9-e8	80	DLM	
$goe^2_OH_2^+ = goe^2_OH + H^+$	-7.38	3.8e-6	80	DLM	1
$goe^2_O^- + H^+ = goe^2_OH$	10.74	3.8e-6	80	DLM	
$goe^1_OCd^+ + H^+ = goe^1_OH + Cd^{+2}$	-1.29	3.9-8	80	DLM	1
$goe^2_OCd^+ + H^+ = goe^2_OH + Cd^{+2}$	1.83	3.8e-6	80	DLM	
$goe^1_OPb^+ + H^+ = goe^1_OH + Pb^{+2}$	-4.78	3.9-e8	80	DLM	1
$goe^2_OPb^+ + H^+ = goe^2_OH + Pb^{+2}$	-1.52	3.8e-6	80	DLM	
$goe^2_H_2AsO_4 + H_2O = goe^2_OH + AsO_4^{+3} + 3H^+$	-31.0	3.32e-6	80	DLM	2
$goe^2_HAsO_4^- + H_2O = goe^2_OH + AsO_4^{+3} + 2H^+$	-26.81	3.32e-6	80	DLM	
Illite					
$ill_OH_2^+ = ill_OH + H^+$	-8.02	2.27e-6	66.8	CCM, κ =2.0 F/m^2	3
$ill_O^- + H^+ = ill_OH$	8.93	2.27e-6	66.8	CCM, κ =2.0 F/m^2	
$ill_OCd^+ + H^+ = ill_OH + Cd^{+2}$	3.62	2.27e-6	66.8	CCM, κ =2.0 F/m^2	3
$(ill_)_2Cd + 2H^+ = 2ill_H + Cd^{+2}$	-0.63	1.3e-6	66.8	CCM, κ =2.0 F/m^2	
$ill_CdOH + 2H^+ = ill_H + Cd^{+2} + H_2O$	6.49	1.3e-6	66.8	CCM, κ =2.0 F/m^2	
$ill_OPb^+ + H^+ = ill_OH + Pb^{+2}$	0.70	2.27e-6	66.8	CCM, κ =2.0 F/m^2	3
$(ill_)_2Pb + 2H^+ = 2ill_H + Pb^{+2}$	-1.37	1.3e-6	66.8	CCM, κ =2.0 F/m^2	
$ill_PbOH + 2H^+ = ill_H + Pb^{+2} + H_2O$	3.65	1.3e-6	66.8	CCM, κ =2.0 F/m^2	
$ill_H_2AsO_3 + H_2O = ill_OH + H_3AsO_3$	-2.12	3.83e-6	66.8	CCM, κ =1.06 F/m^2	4
$ill_HAsO_3^- + H_2O + H^+ = ill_OH + H_3AsO_3$	**5.66**	**3.83e-6**	**66.8**	**CCM, κ =1.06 F/m^2**	

Table 11: Surface sorption reactions for As, Cd, and Pb on goethite, illite, kaolinite, and montmorillonite (DLM = double layer model, CCM = constant capacitance model) (cont.)

Reactions	Log k_{int}	Site Density mol/m^2	Surface Area m^2/g	Type of SCM Model	Reference
Kaolinite					
kao_OH_2^+ = kao_OH + H^+	-4.63	2.24e-6	22.42	CCM, κ =1.2 F/m^2	5
kao_O^- + H^+ = kao_OH	7.54	2.24e-6	22.42	CCM, κ =1.2 F/m^2	
Kao_OCd^+ + H^+ = Kao_OH + Cd^{+2}	3.23	2.24e-6	22.42	CCM, κ =1.2 F/m^2	5
(Kao_)$_2$Cd + 2H^+ = 2Kao_H + Cd^{+2}	-1.22	3.57e-7	22.42	CCM, κ =1.2 F/m^2	
Kao_OPb^+ + H^+ = Kao_OH + Pb^{+2}	0.64	2.24e-6	22.42	CCM, κ =1.2 F/m^2	5
(Kao_)$_2$Pb + 2H^+ = 2Kao_H + Pb^{+2}	-2.36	3.57e-7	22.42	CCM, κ =1.2 F/m^2	
kao_$HAsO_3^-$ + H_2O + H^+ = kao_OH + H_3AsO_3	5.43	3.83e-6	22.42	CCM, κ =1.06 F/m^2	4
kao_AsO_4^{-2} + H_2O + 2H^+ = kao_OH + H_3AsO_4	4.69	3.83e-6	22.42	CCM, κ =1.06 F/m^2	4
Montmorillonite					
mon_OH_2^+ = mon_OH + H^+	-6.04	4.41e-6	46	CCM, κ =3.2 F/m^2	6
mon_O^- + H^+ = mon_OH	6.63	4.41e-6	46	CCM, κ =3.2 F/m^2	
mon_Na^+ + H^+ = mon_H + Na^+	-0.18	1.53e-5	46	CCM, κ =3.2 F/m^2	
mon_OCd^+ + H^+ = mon_OH + Cd^{+2}	2.93	4.41e-6	46	6	6
(mon_)$_2$Cd + 2H^+ = 2mon_H + Cd^{+2}	**-2.37**	**1.53e-5**	**46**	**CCM, κ =3.2 F/m^2**	

Table 11: Surface sorption reactions for As, Cd, and Pb on goethite, illite, kaolinite, and montmorillonite (DLM = double layer model, CCM = constant capacitance model) (cont.)

Reactions	Log k_{int}	Site Density mol/m^2	Surface Area m^2/g	Type of SCM Model	Reference
Montmorillonite					
mon_OPb$^+$ + H$^+$ = mon_OH + Pb^{+2}	-0.49	4.41e-6	46	CCM, κ =3.2 F/m^2	6
(mon_)$_2$Pb + 2H$^+$ = 2mon_H + Pb^{+2}	-2.56	1.53e-5	46	CCM, κ =3.2 F/m^2	
mon_H_2AsO_3 + H_2O = mon _OH + H_3AsO_3	-1.19	3.83e-6	46	CCM, κ =1.06 F/m^2	4
mon_$HAsO_3^-$ + H_2O + H$^+$ = mon _OH + H_3AsO_3	3.92	3.83e-6	46	CCM, κ =1.06 F/m^2	4

1. Swedlund et al. 2009
2. Dixit and Hering, 2003
3. Gu and Evans, 2007
4. Gu and Evans, 2008
5. Gu et al., 2010
6. Goldberg, 2002

4.3 CHEMICAL SCALING FACTOR RESULTS

Goodness of fit was evaluated by comparing scaling factors estimated from the numerical simulations (Equation 4) and the emulations (Equation 5). Correlation coefficients range between R^2 = 0.76 to 0.86 for trace metals and R^2 = 0.52 to 0.66 for the organics (Figures 7 and 8). Improvements in the accuracy of the scaling functions may be achieved by using different mathematical forms for the scaling functions.

Table 12: Correlation coefficients from linear correlations of scaling functions calculated from the simulations and emulations shown in Figures 7 and 8

Parameter	R^2
As	0.795
Ba	0.862
Cd	0.851
Pb	0.757
Benzene	0.662
Naphtalene	0.521
Phenol	0.619

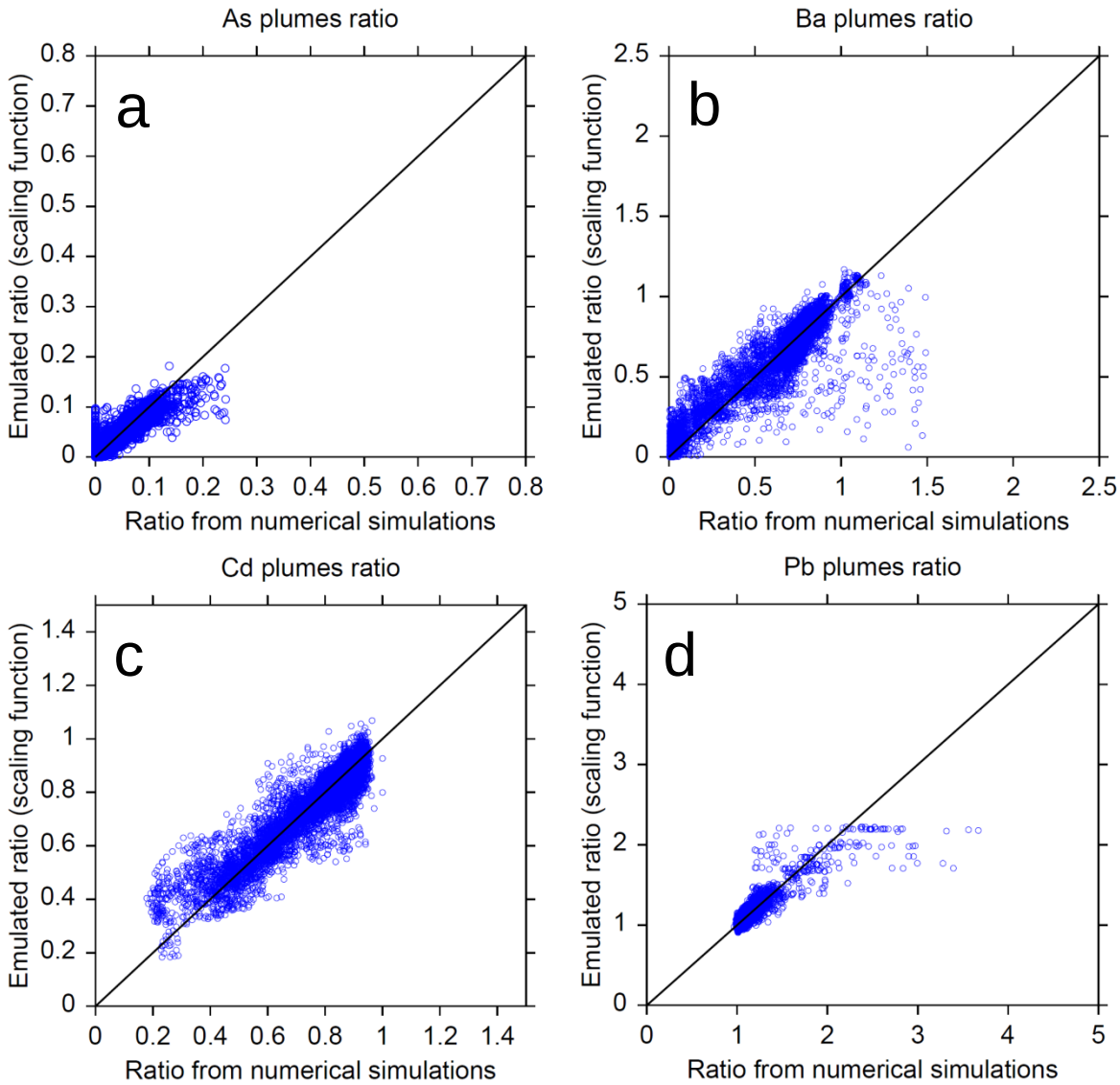

Figure 7: Comparison between the values from numerical simulations and those emulated with the developed scaling functions: As (a), Ba (b), Cd (c), and Pb (d).

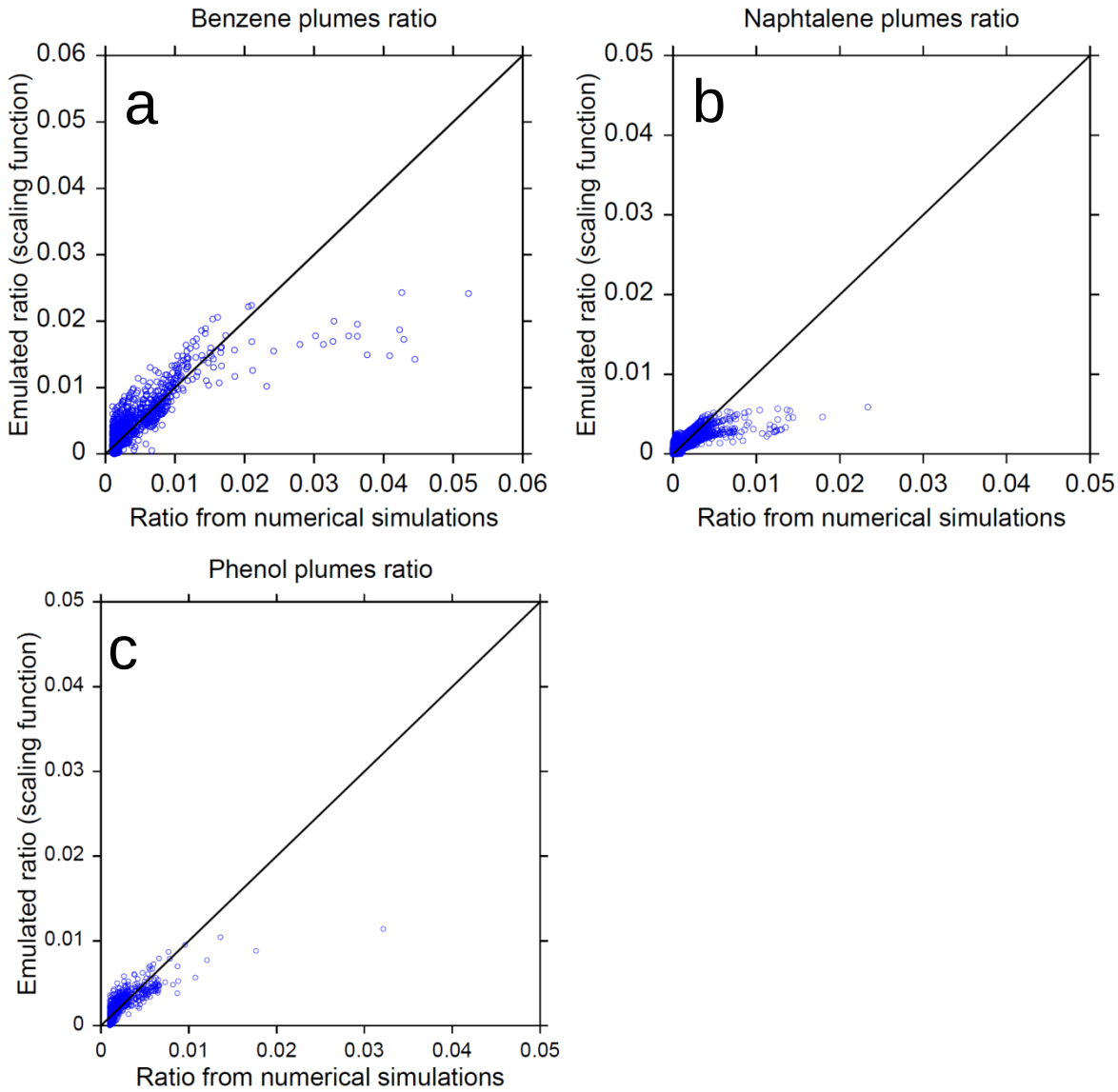

Figure 8: Comparison between the values from numerical simulations and those emulated with the developed scaling functions: benzene(a), naphthalene (b), and phenol (c).

5. RESULTS FROM THE INTEGRATED ROM FOR GROUNDWATER CHEMISTY

Figures 9 and 10 compare plume volumes estimated from the hydrology ROM, which considered the reservoir source term for trace metals and organics, with plume volumes estimated with the scaling function that accounts for the full suite of geochemical reactions. Recall that the hydrology ROM considers variability and uncertainty in the geostatistical model and in CO_2 and brine leakage rates. Inclusion of trace metal chemistry using the scaling function tends to increase plume volumes by about 10 times for As and Ba and 100 times for Cd and Pb, as can be seen by comparing the green and dashed-red cumulative distribution profiles in Figure 9. The results suggest that release of As, Ba, Cd, and Pb from the shallow aquifer sediments as the pH plume advances has a greater footprint than trace metal contamination from the storage reservoir. There are three possible outcomes from this analysis. One is that trace metal leakage sources need not be considered for risk assessments, because their input will be small relative to geochemical reactions within the protected aquifer. The second outcome is that the pH plume volumes derived from the hydrology ROM could be used as proxies for Ba, Cd, and Pb, because their plume volumes are about the same as the pH plume volume, as can be seen by comparing the solid and dashed red lines in Figure 9. This is not the case for As, whose plume was about 10 times smaller than the pH plume. The third outcome is that direct assessment of trace metal release from the aquifer sediment could lower the uncertainty. This can easily be achieved through experiment (Little and Jackson, 2010). It is important to conduct the experiment because of the complexity of the geochemical reactions and uncertainty associated with assessable surface area available for reaction. Direct knowledge of the bulk sediment response to CO_2 saturated waters might allow the trace metal thresholds to be directly correlated to variable pH thresholds.

In contrast to the trace metals, application of the scaling factor $g'(x)$ (see Equation 2) yields large decreases in the organic plume volumes that are attributed to strong bio degradation. Plume sizes are reduced by 10 times for benzene, 100 times for phenol, and 1,000 times for naphthalene. Strong degradation of organics suggests minimal long-term impact of organic constituents.

As mentioned above, scaling functions were not applied to pH and TDS plume volumes, their results from hydrology ROM are shown in Figure 11.

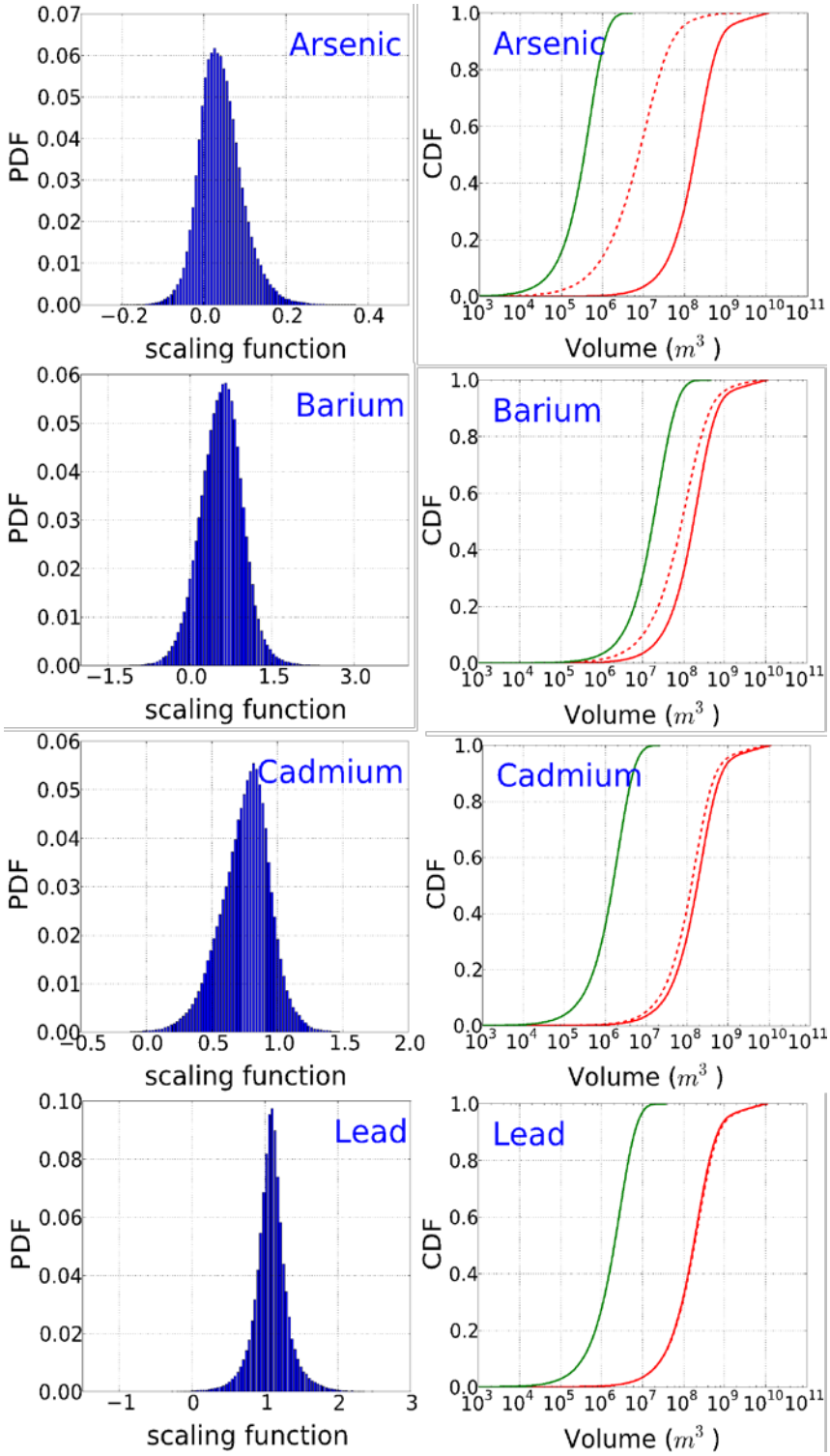

Figure 9: Application of the scaling factors for arsenic, barium, cadmium, and lead (left column) to the hydrology ROM (right column) where the solid green line represents trace metal output from the hydrology ROM, the dashed red line represents the hydrology ROM corrected for geochemical reactions, and the solid red line represents the pH plume volume.

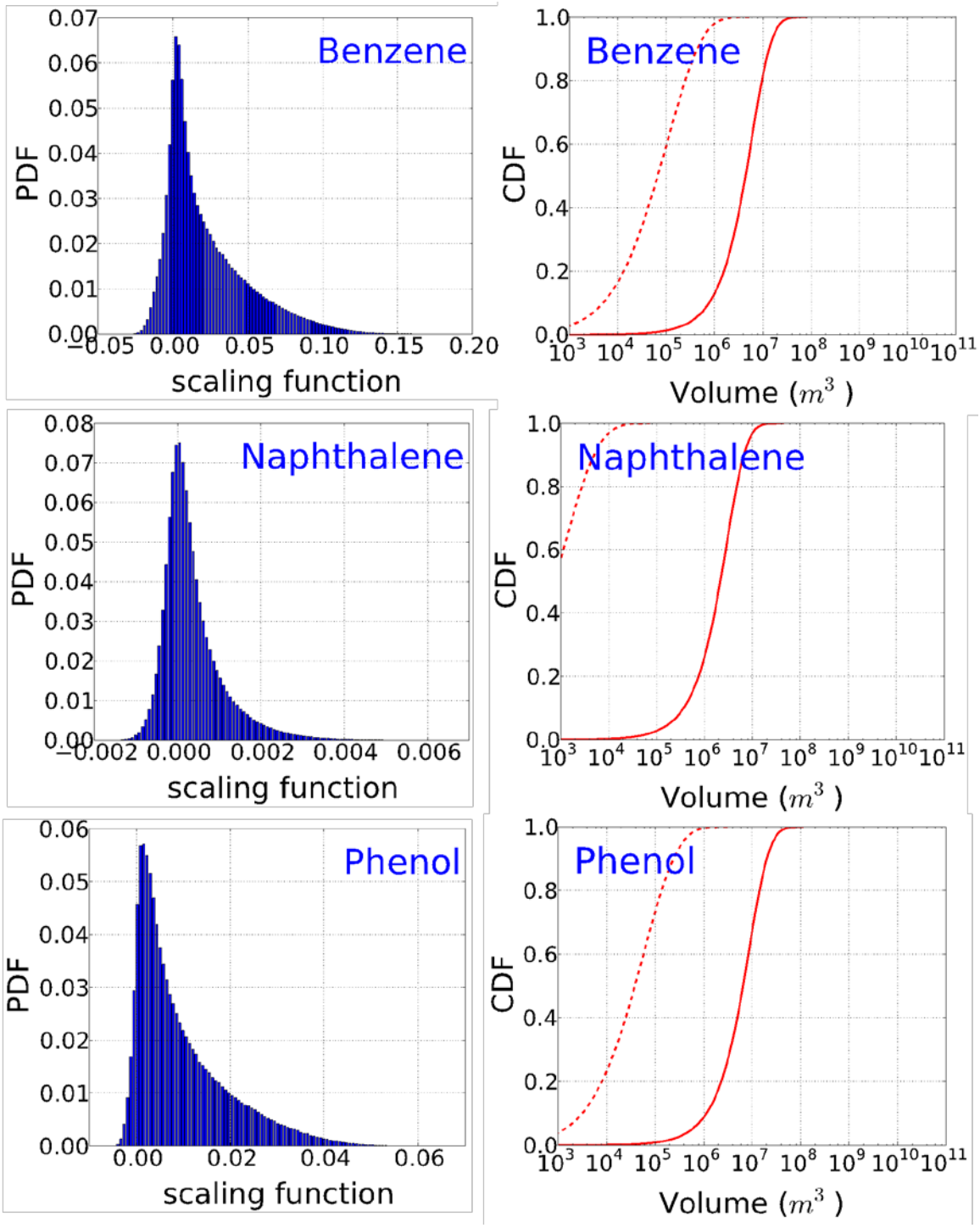

Figure 10: Application of the scaling factors g'(x) (left column) to the hydrology ROM (right column) where the solid and dashed lines represent the uncorrected and corrected plume volumes for benzene, naphthalene, and phenol.

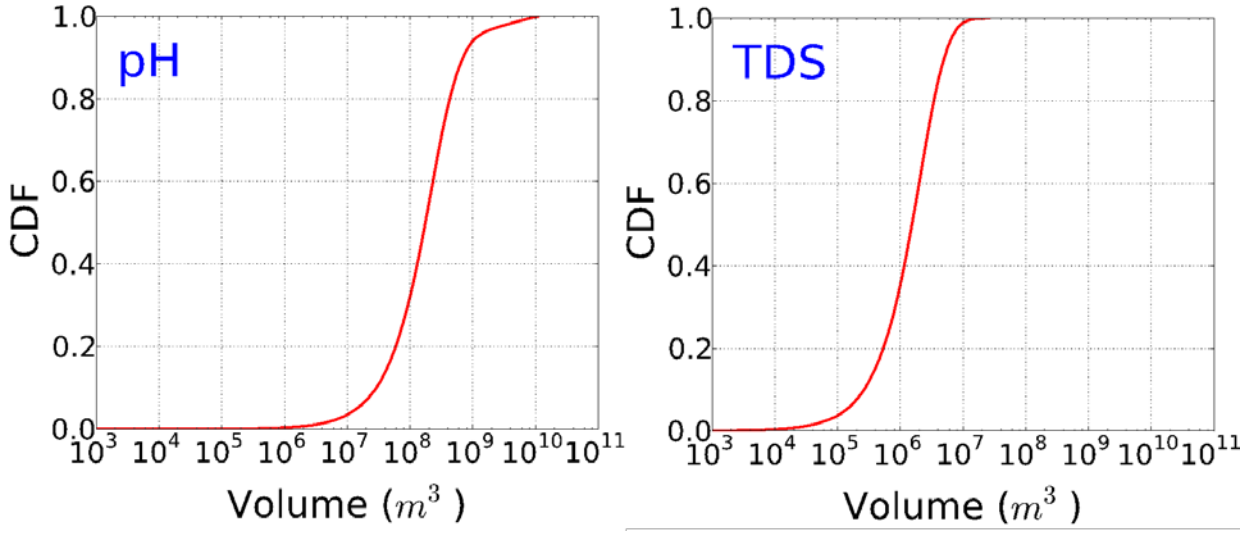

Figure 11: Range of pH and TDS plume volumes estimated from the hydrology ROM.

6. EFFECTS OF WELLBORE MITIGATION ON PLUME VOLUME AND MIGRATION

This project explored the ability of the protected groundwater to return to ambient conditions through natural recharge once leakage source terms have been fixed, because the previous work indicated that CO_2 buoyancy continued to drive leakage and plume growth even after injection stopped and the storage reservoir returned to pre-injection pressures. In these simulations well remediation is implemented by tuning the CO_2 and brine flux to zero. Figure 12 shows the correlations between pH and TDS plume volume and mitigation time for thresholds pH = 7 and TDS = 1,300 mg/l. As was the case in the second-generation results, there is strong correlation between CO_2 mass and pH plume volume with a secondary dependence on mitigation time which also correlates with cumulative leak mass. The correlation for the TDS plume volume on brine mass is more variable than pH volume because the TDS volume is also dependent on brine concentration.

Natural recharge has the potential to remediate changes to groundwater chemistry, but it may take several decades. The effect of well mitigation is illustrated in Figure 13 in plan view for one realization of the plume evolution in which the well is fixed after 42 years of leakage. As is expected, the pH and TDS plumes increase in size as leakage into the aquifer continues between 10 and 40 years (red and orange contours). Once the leaking well has been fixed, the pH plume increases in size and also migrates in the direction of the plume (yellow contour). The larger plume size, in the absence of active leakage, is due to dilution and dispersion of more acid waters within the plume between 40 and 90 years (orange and yellow contours). The pH plume continues to migrate down gradient with no change in volume between 90 and 135 years (yellow and green contours). Eventually natural recharge and dispersion reduce the plume as is evident by slightly smaller area at 200 years (cyan contour).

In contrast to groundwater pH, natural recharge and dispersion have restored groundwater quality to TDS values below the no-impact threshold within 50 years of fixing the leaking well. The much faster recovery of the TDS-impacted groundwater over the pH-impacted groundwater reflects the much higher baseline threshold as well as the modest TDS concentration of the leaking brine (~41,500 mg/l). These two factors result in smaller plumes that are more easily restored. It would be expected that groundwater exposed to more concentrated TDS leaks would exhibit similar plume behavior to that illustrated for pH plumes.

These images of plume evolution show that natural recharge and dispersion have the potential to return groundwater to its pre-leakage condition, but that it can take many years depending on size and concentration of the leak and when it was fixed. They also show that plumes are not static but move in the direction flow. These two findings are relevant to development of groundwater monitoring and remediation plans.

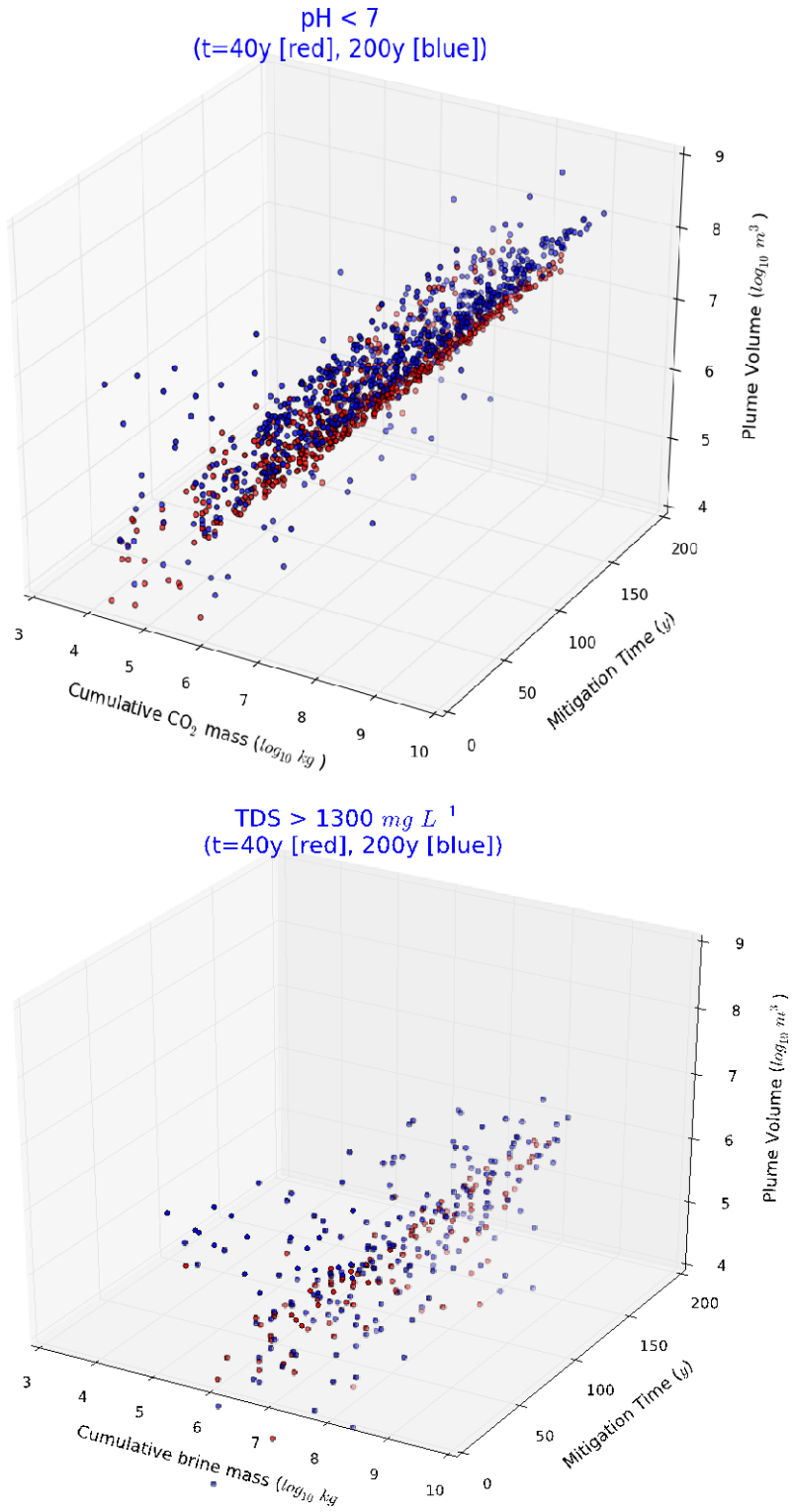

Figure 12: Correlation of pH 7 and TDS 1,300 mg/L volumes with cumulative CO_2 and brine mass and mitigation time.

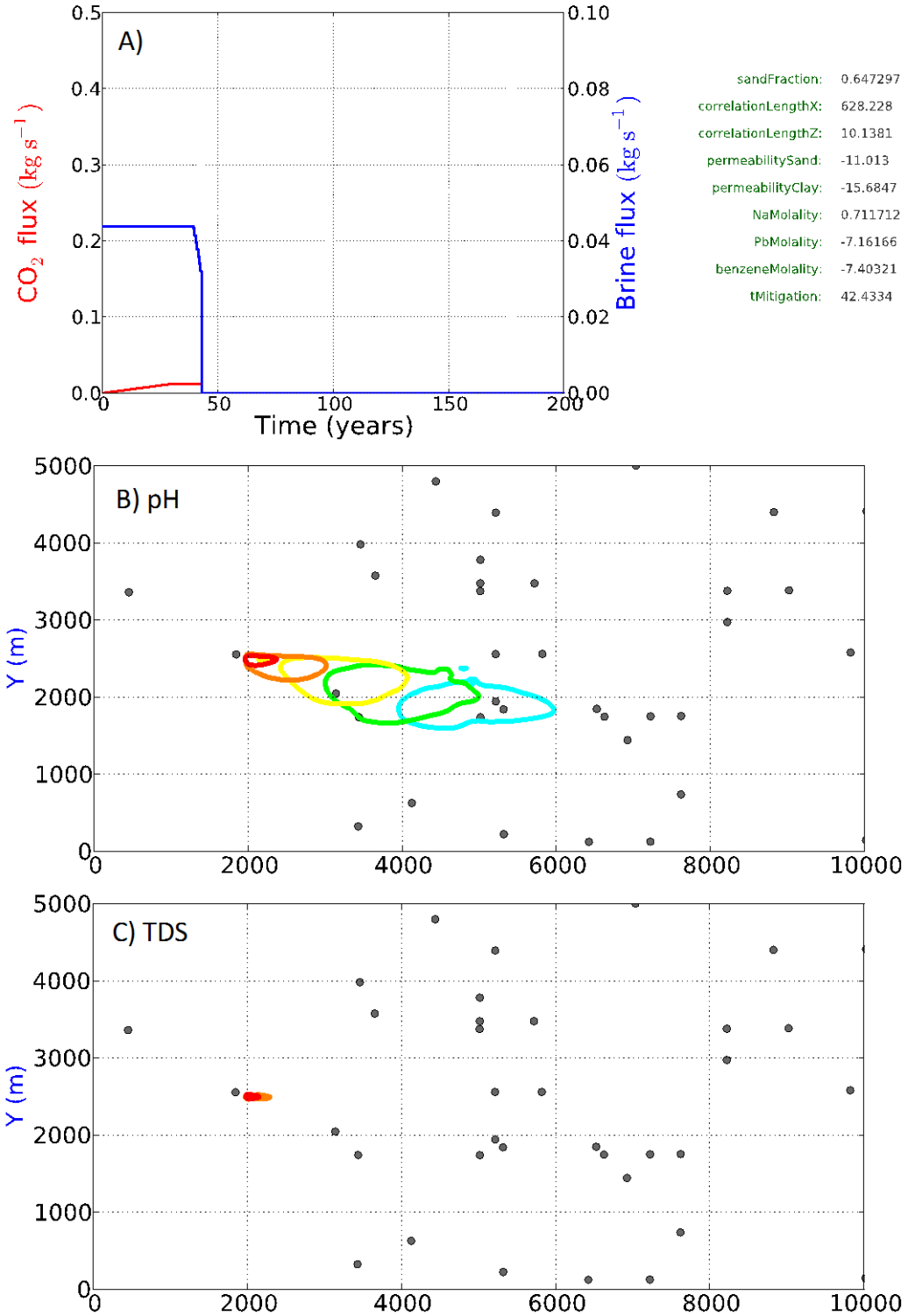

Figure 13: Example of pH (B) and TDS (C) plume evolution in plan view for given simulation (#682) with specific parameter input listed in (A). Color contours correspond to red = 10 years, orange = 40 years, yellow = 90, green = 135 years, cyan = 200 years. Solid circles show the location of shallow groundwater wells at this site.

7. CONCLUSIONS

This study developed ROMs that describe changes in dilute groundwater chemistry if CO_2 and brine were to leak into an overlying alluvium aquifer similar to the High Plains aquifer, Haskel County, Kansas, USA. The protocol allows uncertainty and variability in aquifer heterogeneity, fluid transport, and geochemical reactions to be collectively evaluated to assess potential changes in groundwater pH, TDS, As, Ba, Cd, Pb, benzene, naphthalene and phenol concentrations by developing a scaling function that can be applied to correct the output from hydrology ROM. The chemical scaling function is developed by comparing output from 500 reactive-transport simulations with and without chemistry for simplified 3-D models based on a single representation of aquifer heterogeneity and CO_2 and brine leakage profiles. No correction is needed for pH because calcite dissolution, the most important pH buffering processes, is included in the hydrology ROM. No correction is applied to TDS because calcite dissolution does not change the impacted volume above those predicted by the hydrology ROM. Adsorption and cation exchange are important for trace metal, but have very limited effect on TDS. Inclusion of chemical correction increases trace metal plumes by 10 to 100 times, suggesting that CO_2 leakage leaches trace metals from the aquifer sediments and should be considered in risk assessments. Although more study is needed, as are corrections for other trace metals, such as chromium, iron, manganese, and zinc, the strong correlation of trace metal and pH plume volumes suggests that trace metal impact maybe approximated by pH plumes, greatly simplifying the calculations. In contrast to the observed increases in trace metal plume volumes, inclusion of bio-degradation greatly reduces plume volumes for organics.

Although a general protocol has been established for developing a ROM that can be used to assess groundwater impacts by including physical and chemical uncertainty and variability, there is room for improvement. The model accuracy is not very high when emulations are compared to simulated output. Correlation coefficients range between $R^2 = 0.75$ to 0.85 for trace metals and about 0.60 for the organics. These values are lower than the 0.90 or better goal of the NRAP program. Improvements may be achieved by increasing the number of simulations to more fully sample the parameter space and by applying different mathematical forms for the chemical scaling function.

There is also room for improvement for the hydrology pH and TDS ROMs. Better agreement between the ROMs at times less than 50 years are needed to assess near-term risks to leakage and to evaluate mitigation and monitoring plans. This will require a much finer mesh size to capture changes in groundwater chemistry from small amounts of CO_2 and brine leaked into the aquifer. Smaller mesh sizes may also be needed to improve the overall performance of the TDS ROM. The small TDS plume volumes yield ROMS that are only accurate to about 75% with the current mesh structure.

In order to make ROMs applicable for other alluvium aquifers, this study recommends that ROMs be developed for variable thresholds in light of the “no net degradation” requirement in the U.S. EPA guidelines (2010), because other aquifers are likely to have different background water chemistry. The full chemical and hydrology ROMs developed here are specific to the output thresholds that define no net degradation to the High Plains aquifer. Variable threshold ROMs could be extracted from the same dataset.

8. REFERENCES

Aiuppa, A.; Federico, C.; Allard, P.; Gurrieri, S.; Valenza, M. Trace metal modeling of groundwater-gas-rock interactions in a volcanic aquifer: Mount Vesuvius, Southern Italy. *Chemical Geology* **2005,** *216*, 289–311.

Appelo, C. J. A.; Postma, D. *Geochemistry, groundwater and pollution*; A.A.Balkema: Rotterdam, Netherlands, 1994.

Apps, J. A.; Zheng, L.; Zhang, Z.; Xu, T.; Birkholzer, J. T. Evaluation of potential changes in groundwater quality in response to CO2 leakage from deep geologic storage. Transp. Porous Med. **2010,** *82*, 215–246.

Becker, M. F; Bruce, B. W.; Pope, L. M.; Andrews, W. J. *Ground-Water Quality in the Central High Plains Aquifer, Colorado, Kansas, New Mexico, Oklahoma, and Texas, 1999;* Water-Resources Investigations Report, 02-4112; U.S. Geological Survey, 2002.

Birkholzer, J. T.; Apps, J. A.; Zheng, L.; Zhang, Y.; Xu, T.; Tsang, C.-F. *Research Project on CO2 Geological Storage and Groundwater Resources: Water Quality Effects Caused by CO2 Intrusion into Shallow Groundwater*; Lawrence Berkeley National Laboratory: Berkeley, CA, 2008; p 450.

Blanc, P.; Lassin, A.; Piantone, P.; Azaroual, M.; Jacquemet, N.; Fabbri, A.; Gaucher, E. C. Thermoddem: A geochemical database focused on low temperature water/rock interactions and waste materials. *Applied Geochemistry* **2012,** *27*, 2107–2116.

Carle, S. F. *T-PROGS: Transitional probability geostatistical software users' guide*; University of California, Davis, CA, 1999.

Carroll, S.; Hao, Y.; Aines, R. Geochemical detection of CO_2 in dilute aquifers. *Geochemical Transactions* **2009,** *10*, 4.

Carroll, S. A.; Mansoor, K.; Sun, Y. *Second-Generation Reduced-Order Model for Calculating Groundwater Impacts as a Function of pH, Total Dissolved Solids, and Trace Metal Concentration*; NRAP-TRS-III-002- 2014; NRAP Technical Report Series; U.S. Department of Energy, National Energy Technology Laboratory: Morgantown, WV, 2014; p 40.

Dixit, S.; Hering, J. G. Comparison of Arsenic(V) and Arsenic(III) Sorption onto Iron Oxide Minerals: Implications for Arsenic Mobility. *Environ. Sci. Technol.* **2003,** *37*, 4182–4189.

Forrester, A. I. J.; Sobester, A.; Keane, A. J. Multi-fidelity optimization via surrogate modelling. *Proc. R. Soc. A* **2007,** *463*, 3251–3269.

Goldberg, S. Competitive Adsorption of Arsenate and Arsenite on Oxides and Clay Minerals. *SOIL SCIG SOC. AM. J.* **2002,** *66*, 413–421.

Gu, X.; Evans, L. J. Modelling the adsorption of Cd(II), Cu(II), Ni(II), Pb(II), and Zn(II) onto Fithian illite. *Journal of Colloid and Interface Science* **2007,** *307*, 317–325.

Gu, X.; Evans, L. J. Surface complexation modelling of Cd(II), Cu(II), Ni(II), Pb(II) and Zn(II) adsorption onto kaolinite. *Geochimica et Cosmochimica Acta* **2008,** *72*, 267–276.

Gu, X.; Evans, L. J.; Barabash, S. J. Modeling the adsorption of Cd (II), Cu (II), Ni (II), Pb (II) and Zn (II) onto montmorillonite. *Geochimica et Cosmochimica Acta* **2010,** *74*, 5718–5728.

Hao, Y.; Sun, Y.; Nitao, J. J. Overview of NUFT: a versatile numerical model for simulating flow and reactive transport in porous media. *Groundwater Reactive Transport Models*; Bentham Science Publishers, 2011; pp .213–5728.240.

Huang, D.; Allen, T. T.; Notz, W. I.; Miller, R. A. Sequential kriging optimization using multiple-fidelity evaluations. *Struct. Multidisc. Optim.* **2006,** *32*, 369–382. DOI:10.1007/s00158-005-0587-0

Kharaka, Y. K.; Thordsen, J. J.; Kakouros, E.; Ambats, G.; Herkelrath, W. N.; Beers, S. R.; Birkholzer, J. T.; Apps, J. A.; Spycher, N. F.; Zheng, L.; Trautz, R. C.; Rauch, H. W.; Gullickson, K. S. Changes in the chemistry of shallow groundwater related to the 2008 injection of CO2 at the ZERT field site, Bozeman, Montana. *Environmental Earth Sciences* **2010,** *60*, 273-284.

Kim, H. S.; Koc, M.; Ni, J. A hybrid multi-fidelity approach to the optimal design of warm forming processes using a knowledge-based artificial neural network. *International Journal of Machine Tools & Manufacture* **2007,** *47*, 211–222.

Koch, P. N.; Simpson, T. W.; Allen, J. K.; Mistree, F. Statistical Approximations for Multidisciplinary Optimization: The Problem of Size. *Special Multidisciplinary Design Optimization Issue of Journal of Aircraft* **1999,** *36*, 275–286.

Last, G.V.; Brown, C. F.; Murray, C. J.; Bacon, D. H.; Qafoku, M. P.; Sharma, M.; Jordan, P. D. *Determining threshold values for identification of contamination predicted by reduced order models*; PNNL-22077; Pacific Northwest National Laboratory, Richland, WA, 2013.

Little, M. G.; Jackson, R. B. Potential Impacts of Leakage from Deep CO_2 Geosequestration on Overlying Freshwater Aquifers. *Environmental Science & Technology* **2010,** *44*, 9225–9232.

Madsen, J. I.; Langthjem, M. Multifidelity response surface approximations for the optimum design of diffuser flows. *Optim. Eng.* **2001,** *2*, 453–468.

Nitao, J. J. *User's manual for the USNT module of the NUFT code, version 2 (NP-phase, NC-component, thermal)*; UCRL-MA-130653; Lawrence Livermore National Laboratory, Livermore, CA, 1998.

Palandri, J.; Kharaka, Y. K. *A compilation of rate parameters of water-mineral interaction kinetics for application to geochemical modeling*; USGS Open File report 2004-1068; U.S. Geological Survey, 2004; p 64.

Razavi, S.; Tolson, B. A.; Burn, D. H. Review of surrogate modeling in water resources. *Water Resour. Res.* **2012,** *48*, W07401. DOI:10.1029/2011WR011527

Sonnenthal, E.; Ito, A.; Spycher, N.; Yui, M.; Apps, J.; Sugita, Y.; Conrad, M.; Kawakami, S. Approaches to modeling coupled thermal, hydrological, and chemical processes in the Drift Scale Heater Test at Yucca Mountain. *Int. J. Rock Mech. Min. Sci.* **2005,** *42*, 6987–6719.

Sun, G.; Li, G.; Stone, M.; Li, Q. A two-stage multi-fidelity optimization procedure for honeycomb-type cellular materials. *Comput. Mater. Sci.* **2010,** *49*, 500–511.

Swedlund, P. J.; Webster, J. G.; Miskelly, G. M. Goethite adsorption of Cu(II), Pb(II), Cd(II), and Zn(II) in the presence of sulfate: Properties of the ternary complex. *Geochimica et Cosmochimica Acta* **2009,** *73*, 1548–1562.

Tong, C. *PSUADE User's Manual*; LLNL-SM-407882; Lawrence Livermore National Laboratory, Livermore, CA, 2005.

Tong, C. Self–validated variance–based methods for sensitivity analysis of model outputs. *Reliab. Eng. Syst. Safe.* **2010,** *95*, 301–309.

Trautz, R. C.; Pugh, J. D.; Varadharajan, C.; Zheng, L.; Bianchi, M.; Nico, P. S.; Spycher, N. F.; Newell, D. L.; Esposito, R. A.; Wu, Y.; Dafflon, B.; Hubbard, S. S.; Birkholzer, J. T. Effect of Dissolved CO2 on a Shallow Groundwater System: A Controlled Release Field Experiment. *Environ. Sci.Technol.* **2012,** *47*, 298-305.

EPA. Code of Federal Regulations, 40 CFR Part 141 and 143, EPA 816-F-09-0004, 2009.

EPA. *Federal requirements under the underground injection control (UIC) Program for carbon dioxide (CO_2) geologic sequestration (GS) Wells*; Technical Report; U.S. Environemntal Protection Agency, 2010.

Viana, F. A. C.; Steffen, V. Jr.; Butkewitsch, S.; Leal, M. D. F. Optimization of aircraft structural components by using nature-inspired algorithms and multi-fidelity approximations, J. Global Optim. **2009,** *45*, 427–449.

Wilkin, R. T.; Digiulio, D. C. Geochemical Impacts to Groundwater from Geologic Carbon Sequestration: Controls on pH and Inorganic Carbon Concentrations from Reaction Path and Kinetic Modeling. *Environmental Science & Technology* **2010,** *44*, 4821–4827.

Wolery, T. J. *EQ3/6, A software package for geochemical modelling of aqueous systems, Version 7.2*; Lawrence Livermore National Laboratory: Livermore, CA, 1993.

Xu, T.; Sonnenthal, E.; Spycher, N.; Pruess, K. TOUGHREACT: A Simulation Program for Non-isothermal Multiphase Reactive Geochemical Transport in Variably Saturated Geologic Media. *Computers and Geosciences* **2006,** *32*, 145–165.

Zheng, L.; Apps, J. A.; Zhang, Y.; Xu, T.; Birkholzer, J. T. On mobilization of lead and arsenic in groundwater in response to CO_2 leakage from deep geological storage. *Chemical geology* **2009,** *268*, 281–297.

Zheng, L.; Spycher, N.; Birkholzer, J. T.; Xu, T.; Apps, J.; Kharaka, Y. *Modeling studies on the transport of benzene and H_2S in CO_2-water systems*; Technical Report: LBNL-4339E; Lawrence Berkeley National Laboratory: Berkeley, CA, 2010.

Zheng, L.; Apps, J. A.; Spycher, N.; Birkholzer, J. T.; Kharaka, Y. K.; Thordsen, J.; Beers, S. R.; Herkelrath, W. N.; Kakouros, E.; Trautz, R. C. Geochemical modeling of changes in shallow groundwater chemistry observed during the MSU-ZERT CO2 injection experiment. *International Journal of Greenhouse Gas Control* **2012,** *7*, 202–217.

NRAP is an initiative within DOE's Office of Fossil Energy and is led by the National Energy Technology Laboratory (NETL). It is a multi-national-lab effort that leverages broad technical capabilities across the DOE complex to develop an integrated science base that can be applied to risk assessment for long-term storage of carbon dioxide (CO_2). NRAP involves five DOE national laboratories: NETL, Lawrence Berkeley National Laboratory (LBNL), Lawrence Livermore National Laboratory (LLNL), Los Alamos National Laboratory (LANL), and Pacific Northwest National Laboratory (PNNL).

Technical Leadership Team

Diana Bacon
Lead, Groundwater Protection Working Group
Pacific Northwest National Laboratory
Richmond, WA

Jens Birkholzer
LBNL Lab Lead
Lawrence Berkeley National Laboratory
Berkeley, CA

Grant Bromhal
Technical Director, NRAP
Research and Innovation Center
National Energy Technology Laboratory
Morgantown, WV

Chris Brown
PNNL Lab Lead
Pacific Northwest National Laboratory
Richmond, WA

Susan Carroll
LLNL Lab Lead
Lawrence Livermore National Laboratory
Livermore, CA

Abdullah Cihan
Lead, Reservoir Performance Working Group
Lawrence Berkeley National Laboratory
Berkeley, CA

Tom Daley
Lead, Strategic Monitoring Working Group
Lawrence Berkeley National Laboratory
Berkeley, CA

Robert Dilmore
NETL Lab Lead
Research and Innovation Center
National Energy Technology Laboratory
Pittsburgh, PA

Nik Huerta
Lead, Migration Pathways Working Group
Research and Innovation Center
National Energy Technology Laboratory
Albany, OR

Rajesh Pawar
LANL Lab Lead
Lead, Systems/Risk Modeling Working Group
Los Alamos National Laboratory
Los Alamos, NM

Tom Richard
Deputy Technical Director, NRAP
The Pennsylvania State University
State College, PA

Josh White
Lead, Induced Seismicity Working Group
Lawrence Livermore National Laboratory
Livermore, CA

Sean Plasynski
Executive Director
Technology Development and Integration Center
National Energy Technology Laboratory
U.S. Department of Energy

Heather Quedenfeld
Associate Director
Coal Development and Integration
National Energy Technology Laboratory
U.S. Department of Energy

Traci Rodosta
Technology Manager
Strategic Planning
Science and Technology Strategic Plans and Programs
National Energy Technology Laboratory
U.S. Department of Energy

Mark Ackiewicz
Director
Division of Carbon Capture and Storage
Office of Fossil Energy
U.S. Department of Energy

NRAP Executive Committee

Cynthia Powell
Executive Director
Research and Innovation Center
National Energy Technology Laboratory

Donald DePaolo
Associate Laboratory Director
Energy and Environmental Sciences
Lawrence Berkeley National Laboratory

Roger Aines
Chief Energy Technologist
Lawrence Livermore National Laboratory

Melissa Fox
Program Manager
Applied Energy Programs
Los Alamos National Laboratory

George Guthrie
Chair, NRAP Executive Committee
Earth and Environmental Sciences
Los Alamos National Laboratory

Alain Bonneville
Laboratory Fellow
Pacific Northwest National Laboratory

Grant Bromhal
Technical Director, NRAP
Senior Research Fellow
Research and Innovation Center
National Energy Technology Laboratory

NRAP Technical Report Series